Lithos 382–383 (2021) 105959

Contents lists available at ScienceDirect

Lithos

journal homepage: www.elsevier.com/locate/lithos

Research Article

Major-trace element and Sr-Nd isotope compositions of mafic dykes of the Singhbhum Craton: Insights into evolution of the lithospheric mantle

Om Prakash Pandey [a,b,*], Klaus Mezger [a], Dewashish Upadhyay [c], Debajyoti Paul [b], Ajay Kumar Singh [c], Ulf Söderlund [d,e], Ashley Gumsley [d,f]

[a] Institute of Geological Sciences, University of Bern, Baltzerstrasse 1+3, 3012 Bern, Switzerland
[b] Department of Earth Sciences, Indian Institute of Technology Kanpur, Kanpur 208016, India
[c] Department of Geology and Geophysics, Indian Institute of Technology Kharagpur, Kharagpur 721302, India
[d] Department of Geology, Lund University, Sölvegatan 12, SE-223 62 Lund, Sweden
[e] Department of Geosciences, Swedish Museum of Natural History, SE-10405 Stockholm, Sweden
[f] Institute of Earth Sciences, University of Silesia in Katowice, Katowice, Poland

ARTICLE INFO

Article history:
Received 21 September 2020
Received in revised form 5 December 2020
Accepted 22 December 2020
Available online 28 December 2020

Keywords:
Dyke swarm
Indian Shield
Large Igneous Provinces
Neoarchean
Paleoproterozoic
SCLM

ABSTRACT

The Singhbhum Craton in eastern India is host to at least seven sets of mafic dyke swarms. Four previously dated swarms (studied here) include the NNE-trending Keshargaria (ca. 2.80 Ga) and Ghatgaon (ca. 2.76 - 2.75 Ga) swarms, the ENE-trending Kaptipada swarm (ca. 2.26 Ga), and the ESE-trending Pipilia swarm (ca.1.76 Ga). The dykes range in composition from basalt to andesite and have transitional tholeiitic to calc-alkaline affinities. They show intra- and inter-swarm geochemical and Sr-Nd isotopic heterogeneities and have SiO_2 content ranging from 47 to 60 wt.%. The chondrite normalized REE patterns show enrichment in LREE and the Primitive-Mantle normalized multi-element patterns show elevated U, Th, Cs, Rb, K, and Pb; and depletion in Nb, Ta, and Ti. These characteristics indicate involvement of crustal component in the petrogenesis of these dykes. The dykes of different swarms have variable $^{87}Sr/^{86}Sr_i$ and $\varepsilon_{Nd(i)}$ values, which define a crust-like isotopic growth trajectory with time from a common chondritic to depleted source that was enriched contemporaneously with the formation of the crustal rocks of the Singhbhum Craton. The isotope data indicate involvement of older enriched crustal material in the petrogenesis of these dykes. Variable but mostly high (compared to similarly evolved magmas) Ni (40 - 590 ppm), Cr (40 - 1110 ppm), and V (120 - 434 ppm) contents particularly of the most primitive dykes indicate that parental melts were in equilibrium with mantle peridotite and experienced only minor fractional crystallization of olivine, pyroxene, and magnetite. The Sr-Nd isotope ratios do not show any correlation with differentiation indices which indicates that the melts were not modified significantly by crustal assimilation during ascent and emplacement. The crust-like secular trend of the Sr and Nd isotopic compositions suggests that the enriched crustal material was incubated in the mantle (i.e., metasomatized lithospheric mantle) for a long time and this source was periodically tapped leading to multiple dyke emplacement events over at least 1 Gyr. The recycled crustal material played a role in metasomatizing the subcontinental lithospheric mantle prior to ca. 2.80 Ga. Mantle plume activity triggered melting of the metasomatized lithospheric mantle many times, leading to the emplacement of mafic dykes of different generations across the craton.

1. Introduction

Mafic dyke swarms are widespread in many Archean cratons of the world and manifest extentionsal events in Earth's history (Ernst, 2014). Although most are of Proterozoic age, the older ones have ages upto Mesoarchean (Ernst, 2014; Gumsley et al., 2015; Halls, 1982). Giant dyke swarms represent the magmatic feeder plumbing system of Large Igneous Provinces (LIPs), which usually are the manifestations of plume events in geological history (e.g., Bryan and Ernst, 2008; Buchan and Ernst, 2018; Ernst and Buchan, 2001; Halls, 1982; Sensarma et al., 2013). The attitude of the dykes is controlled by the regional stress field, with the dykes commonly oriented normal to the regional minimum principal stress direction (Anderson, 1951). However, some dyke swarms form prominent radial arrays emanating from a single point (e.g., the Mackenzie Dyke Swarm; Ernst and Baragar, 1992).

* Corresponding author at: Department of Earth Sciences, Indian Institute of Technology Kanpur, Kanpur 208016, India
E-mail addresses: ompandey@iitk.ac.in, pandeygly@gmail.com (O.P. Pandey).

https://doi.org/10.1016/j.lithos.2020.105959

Dyke swarms are the remnants of the plumbing systems of voluminous mantle-derived magmas and hence can provide important constraints on the nature, history and composition of their mantle source. They represent a time-record of mantle-derived magmatism (e.g., Bleeker, 2004) and can therefore constrain the temporal evolution of the mantle composition (e.g., Bartels et al., 2015; de Kock et al., 2014; Kumar and Rathna, 2008; Wang et al., 2004). Different geochemical reservoirs and processes can contribute to their petrogenesis. These include, (i) delaminated subcontinental lithospheric mantle (SCLM) recycled into the asthenosphere (e.g., Zindler and Hart, 1986), (ii) metasomatically enriched asthenospheric mantle (e.g., Aldanmaz et al., 2006), (iii) thermal boundary layer enriched by mantle plume/asthenospheric melts (e.g., Hasse et al., 2004; Thompson et al., 2005), (iv) SCLM metasomatized by mantle plumes (e.g., Chandra et al., 2019), and (v) SCLM enriched by subduction of crustal material (e.g., Goodenough et al., 2002; Paul et al., 2020; Zhao and McCulloch, 1993).

Dykes of different generations, orientations and compositions are prominent features in all Archean cratons of the Indian Shield (viz. Aravalli, Bundelkhand, Singhbhum, Bastar, and Dharwar Cratons) (e.g., French and Heaman, 2010; Kumar et al., 2017; Pandey et al., 2020; Pradhan et al., 2012; Ratre et al., 2010; Srivastava et al., 2019). In the Singhbhum Craton in eastern India, several early-Neoarchean to late-Paleoproterozoic mafic dyke swarms have intruded into the Paleoarchean to Mesoarchean granitoid crust (e.g., Bose, 2009; Kumar et al., 2017; Roy et al., 2004; Saha, 1994; Sarkar et al., 1969; Shankar et al., 2014; Srivastava et al., 2019). These are collectively referred to as the "Newer Dolerite Dykes" in the literature (e.g., Bose, 2009; Roy et al., 2004; Saha, 1994; Sarkar et al., 1969). Recently, Srivastava et al. (2019) grouped them into seven distinct swarms (Fig. 1). In this study, we report new whole-rock major- and trace-element abundances and Sr-Nd isotope compositions of four previously dated mafic dyke swarms (the ca. 2.80 Ga Keshargaria, ca. 2.76 – 2.75 Ga Ghatgaon, ca. 2.26 Ga Kaptipada, and the ca. 1.76 Ga Pipilia swarms; Kumar et al., 2017; Shankar et al., 2014; Srivastava et al., 2019). The geochemical and isotopic data provide insights into the source of the magmas and secular evolution of their mantle source.

2. Regional geology and previous studies on dykes of the Singhbhum Craton

The Singhbhum cratonic nucleus is dominated by Paleoarchean to Mesoarchean (3.45 - 3.05 Ga) tonalite-trondhjemite-granodiorite (TTG) suites and granites, and greenstone belt successions outcropping along the eastern, western, and southern peripheries of the craton (e.g., Pandey et al., 2019; Upadhyay et al., 2014, 2019). The greenstone belts comprise mafic/ultramafic and minor felsic volcanic rocks intercalated with quartzites, banded iron formations, cherts, schists, and phyllites (e.g., Mukhopadhyay, 2001; Saha, 1994).

The dyke swarms of the Singhbhum Craton are easily visible in satellite images (ESM-Fig. 1). They occur throughout the craton, but are concentrated in the TTGs and gneisses. Although several orientations can be delineated, dykes trending NNE-SSW to NE-SW are prominent (Fig. 1). The most common rock types are quartz dolerite with local occurrences of norite, and subordinate granophyre, syenodiorite, perknite (i.e., lime-magnesia-silicate rocks, composed chiefly of monoclinic amphibole and monoclinic pyroxene), and serpentinised peridotite (Saha, 1994). The characteristic rock-forming minerals of the doleritic dykes are plagioclase, clinopyroxene, orthopyroxene, and minor quartz, magnetite, and ilmenite (e.g., Kumar et al., 2017; Sengupta et al., 2014; Sengupta and Ray, 2012; Shankar et al., 2018; Srivastava et al., 2019).

Srivastava et al. (2019) divided the Neoarchean-Paleoproterozoic mafic dykes into seven distinct swarms, based on their orientations, cross-cutting relationships, and their U-Pb/Pb-Pb baddeleyite ages. These are (1) ca. 2.80 Ga NNE-SSW to NE-SW trending Keshargaria swarm, (2) ca. 2.76 - 2.75 Ga NNE-SSW to NE-SW-trending Ghatgaon swarm, (3) early-Paleoproterozoic E-W to ENE-WSW-trending Keonjhar swarm, (4) ca. 2.26 Ga NE-SW to ENE-WSW-trending Kaptipada swarm, (5) middle-Paleoproterozoic NW-SE to NNW-SSE-trending Bhagamunda swarm, (6) ca. 1.76 Ga WNW-ESE-trending Pipilia swarm, and (7) late-Paleoproterozoic N-S to NNE-SSW-trending Barigaon swarm (Fig. 1). The two oldest swarms, the Keshargaria and Ghatgaon swarms, were dated by Kumar et al. (2017). They reported Pb-Pb baddeleyite thermal extraction – thermal ionization mass spectrometry (TE-TIMS) ages of 2800 ± 1 Ma for the Keshargaria swarm, and 2762 ± 2 Ma and 2752 ± 1 Ma for the Ghatgaon swarm. The Kaptipada swarm dated recently by Srivastava et al. (2019) yielded a U-Pb baddeleyite ID-TIMS (isotope dilution-TIMS) age of 2256 ± 6 Ma. Shankar et al. (2014) reported a Pb-Pb baddeleyite TE-TIMS age of 1765 ± 1 Ma for the Pipilia Swarm. The emplacement ages of the Keonjhar, Bhagamunda, and the Barigaon swarms, remain unknown and their ages are constrained solely based on their orientations and cross-cutting relationships (Srivastava et al., 2019).

Using paleomagnetic constraints and coeval ages of the Ghatgaon swarm (2.76 - 2.75 Ga) from the Singhbhum Craton with mafic magmatic intrusions in the Pilbara and Kaapvaal Cratons, Kumar et al. (2017) proposed that the three cratons were proximal to each other at ca. 2.77 Ga. Additionally, Shankar et al. (2018) suggested that the Singhbhum, North China, and Baltica Cratons were in close spatial proximity at ca. 1.76 Ga, based on the paleomagnetic pole of the 1.76 Ga Pipilia swarm. The ca. 2.26 Ga Kaptipada and the ca. 1.76 Ga Pipilia swarms had been argued to correlate with the 2.26 - 2.25 Ga Ippaguda-Dhiburahalli and ca. 1.78 Ga Pebbair swarms of the Eastern Dharwar Craton, implying that these two crustal blocks were neighbors during this time interval (Srivastava et al., 2019).

3. Materials and methods

A total of 40 samples were collected from the Keshargaria (ca. 2.80 Ga), Ghatgaon (ca. 2.76 Ga), Kaptipada (ca. 2.26 Ga), and the Pipilia (ca. 1.76 Ga) mafic dyke swarms of the Singhbhum Craton (Fig. 1). The sample locations and the nature of geochemical analyses conducted on each are provided in Table 1. In the field, the dykes do not show any discernible zoning in mineral assemblages or grain sizes. Representative photomicrographs of the dyke samples are presented in ESM-Fig. 2. All samples are fine- to medium-grained and commonly display ophitic texture. Major rock-forming minerals include clino- and orthopyroxene, and plagioclase, which show varying degrees of alteration. The accessory phases include quartz, apatite, and Fe-Ti oxides. There is no evidence for xenocrysts or large phenocrysts; all minerals have similar grain sizes, indicating that these dykes represent melt compositions.

3.1. Sample preparation for the whole-rock major- and trace-element analyses

Samples were cleaned and the weathered/altered crusts were removed using a diamond saw. This was followed by washing with water and air-drying in the laboratory. They were crushed in a steel jaw crusher and pulverized using an agate mortar. The homogeneous powders were used to determine whole-rock major- and trace-element concentrations, as well as Rb-Sr and Sm-Nd isotope compositions. Major- and trace-elements were analyzed by Actlabs Canada (package code: 4 Lithoresearch). Samples were fused with lithium metaborate/tetraborate and dissolved in weak (5%) HNO_3. The major and some trace elements (i.e., Sc, V, Sr, Zr, and Ba) were analyzed using an Agilent 700 Series inductively coupled plasma optical emission spectrometer (ICP-OES); all other trace elements were analyzed on a Perkin Elmer SCIEX™ ELAN® 6000 inductively coupled plasma mass spectrometer (ICP-MS). Three blanks and five standards (three before and two after) were analyzed per group of samples for quality control. The precision and accuracy of elemental concentrations measured for certified reference materials (CRMs) were better than 5% for most elements. Measured data for CRMs are listed in ESM-Table 1.

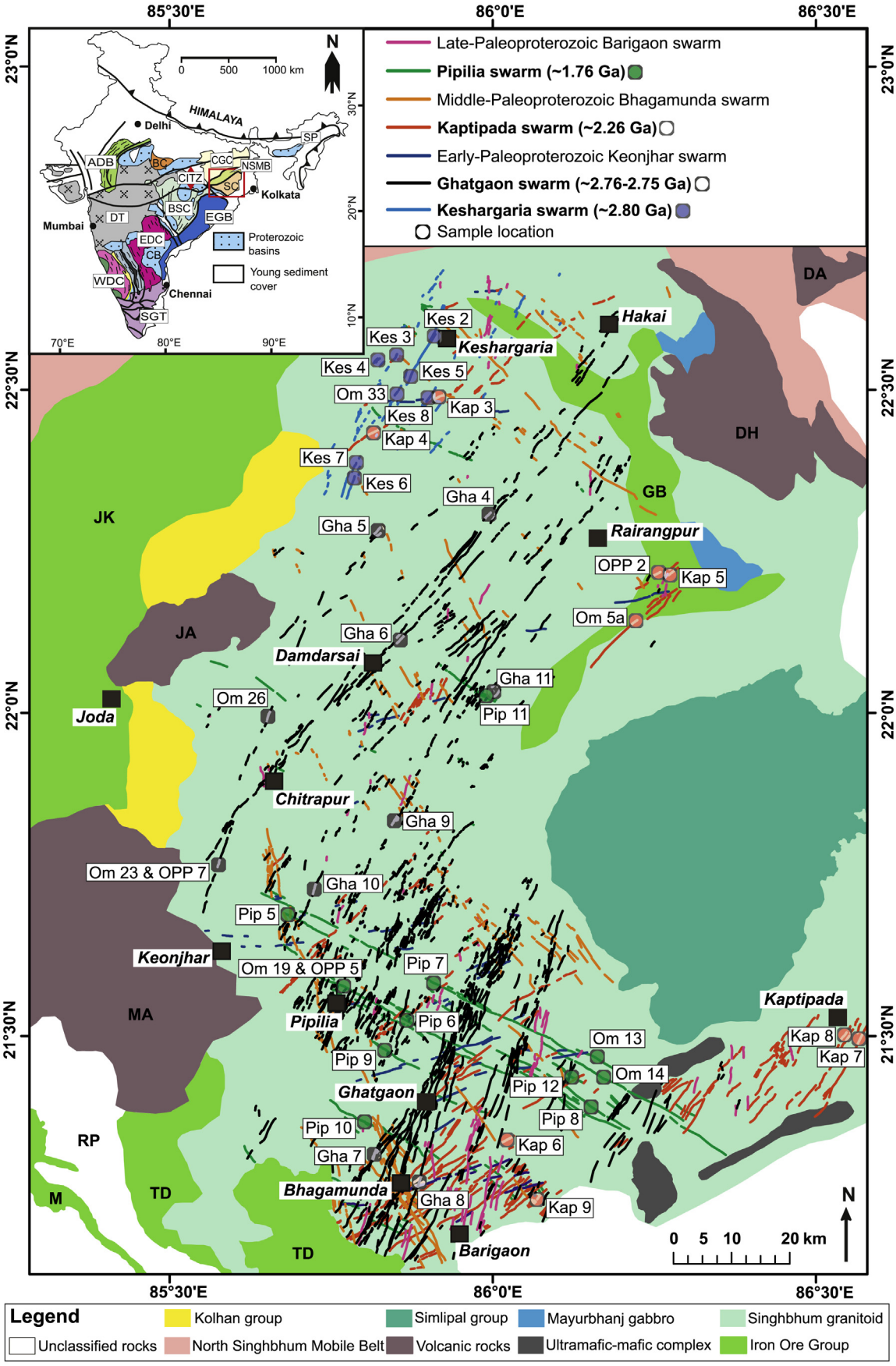

Fig. 1. Geological map of the Singhbhum Craton (modified after Srivastava et al., 2019) showing sample locations marked with solid circles (abbreviations: DA = Dalma, DH = Dhanjori, GB = Gorumahishani-Badampahar, JA = Jagannathpur, JK = Jamda-Koira, M = Malayagiri, MA = Malangtoli, RP = Rengali Province, TD = Tomka-Daitari). The inset map (modified after Upadhyay et al., 2019) is a simplified geological map of India showing different Indian cratons (Singhbhum Craton marked by a red rectangle) and other major geological units (ADB = Aravalli-Delhi Belt, BC = Bundelkhand Craton, DT = Deccan Traps, CITZ = Central Indian Tectonic Zone, CGC = Chhotanagpur Gneiss Complex, SP = Shillong Plateau, SC = Singhbhum Craton, EGB = Eastern Ghats Belt, BSC = Bastar Craton, WDC = Western Dharwar Craton, EDC = Eastern Dharwar Craton, CB = Cuddapah Basin, SGT = Southern Granulite Terrane).

3.2. Whole-rock Rb-Sr and Sm-Nd isotopic analyses

Sample preparation and ion-exchange chromatographic separation procedures for Rb-Sr and Sm-Nd were performed following Pandey et al. (2020). The isotopic measurements were done at the Institute of Geological Sciences, University of Bern, Switzerland. The isotopes of Rb, Sr, and Sm in the spiked samples were measured on a Thermo Scientific™, Neptune Plus™ multicollector ICP-MS (MC-ICP-MS). Neodymium isotopes were measured on a Thermo Scientific™, Triton Plus™ TIMS. Total procedural blanks for all the elements were < 700 pg (i.e., <0.15% of the sample amount). Rubidium and Sm isotope ratios were corrected for mass bias (using the exponential law) by the standard-sample bracketing method with measured JMC Rb and Sm reference materials. After purification, the Sr cuts were dried and diluted to concentration of ~150 ppb (^{88}Sr signal = ~6 V) in 0.5 M HNO_3 for measurement on the MC-ICP-MS. The baselines were measured as 'on-peak zero' (i.e., signals for Sr isotopes and ^{85}Rb were measured in blank 0.5 M HNO_3 and subtracted from the respective signals obtained from the sample/standard measurements) to account for the interference of ^{84}Kr and ^{86}Kr (impurity in Ar) on ^{84}Sr and ^{86}Sr, respectively. The purified Nd fractions were dried and loaded on zone-refined Re filaments (double filament assembly) with 6.4 M HCl for measurement on TIMS. Since the samples were spiked, Nd and Sr isotope ratios were corrected for mass-dependent fractionation using the exponential law and the iteration method suggested by Stracke et al. (2014). Isotope ratios of Nd and Sr isotopic standards JNdi-1 and NIST SRM® 987 were measured for quality control. The measured isotopic ratios of Nd and Sr for the respective standards were corrected for mass fractionation using the exponential law with normalization ratios of $^{146}Nd/^{144}Nd = 0.7219$ and $^{86}Sr/^{88}Sr = 0.1194$, respectively. Standards JNdi-1 and NIST SRM® 987 yielded $^{143}Nd/^{144}Nd = 0.512067 \pm 0.000009$ (2σ; n = 26) and $^{87}Sr/^{86}Sr = 0.710254 \pm 0.000029$ (2σ; n = 15), respectively. Mass bias corrected Nd and Sr isotope ratios of the samples were adjusted with respect to the recommended values for JNdi-1 ($^{143}Nd/^{144}Nd = 0.512115$; Tanaka et al., 2000) and NIST SRM® 987 ($^{87}Sr/^{86}Sr = 0.710245$). The adjustment factors for $^{143}Nd/^{144}Nd$ and $^{87}Sr/^{86}Sr$ were 93.7 ppm [$^{143}Nd/^{144}Nd_{adjustment\ factor} = \{(0.512115 - 0.512067)/0.512115\} \times 10^6 = 93.7$ ppm] and -12.7 ppm [$^{87}Sr/^{86}Sr_{adjustment\ factor} = \{(0.710245 - 0.710254)/0.710245\} \times 10^6 = -12.7$ ppm], respectively.

4. Results

4.1. Whole-rock major- and trace-element geochemistry

The whole-rock major- and trace-element compositions and normative mineralogy of all 40 samples are listed in Table 2 and shown in Figures 2 to 4. The dykes display significant variations in composition and plot in the fields of basalt, basaltic-andesite, and andesite (Figs. 2a, b). They have tholeiitic to calc-alkaline affinities (Fig. 2c). Their SiO_2 content ranges from 47 to 60 wt.% and the Mg# [molar Mg×100/(Mg+Fe)] from 38 to 78 (Table 2; Fig. 3a). The dykes display inter- and intra-swarm chemical heterogeneities (Figs. 2-4, Table 2). Samples from a single swarm or all swarms together do not show well-defined correlations of major- and trace-element against Mg# in bivariate diagrams (Figs. 3a-n). However, most of the samples from the four swarms exhibit negative correlations, albeit poor, for Al_2O_3, FeO(T), Na_2O, TiO_2, P_2O_5, V, and Zr against Mg#; whereas Ni and Cr are positively correlated with Mg#. The dykes have variable concentrations of compatible elements like Ni (40-590 ppm), Cr (40-1110 ppm), and V (120-434 ppm) and these elements are particularly high in the more mafic samples. In Th/Yb vs. Nb/Yb diagram (Fig. 3o; after Pearce, 2008), samples from all four swarms plot above the MORB (mid ocean ridge basalt) - OIB (ocean island basalt) array towards the upper continental crust (UCC) and fall in the field of "arc-basalts" in Th-Zr-Nb tectonic discrimination diagram (Fig. 3p; after Wood, 1980). Most dyke samples (except Kes 8 of the ca. 2.80 Ga swarm, and Pip 9 of the ca. 1.76 Ga swarm) are quartz normative (CIPW norm; calculation steps after Johannsen, 1931) and have variable normative hypersthene and diopside (Table 2). Only samples from two dykes (Kes 8 and Pip 9) are olivine normative.

The chondrite-normalized rare earth element (REE) patterns (Figs. 4a-d) for most of the dyke samples are moderately fractionated with enrichment in the light REE (LREE) and no heavy REE (HREE) fractionation (except for the ca. 1.76 Ga dykes). The LREE show varying degrees of enrichment with a tendency towards ocean island basalt (OIB) and continental crust. The samples with least fractionated REE patterns in each swarm include Kes 8 of the ca. 2.80 Ga swarm; Gha 5 and Gha 11 of the ca. 2.76 Ga swarm; Kap 3, Kap 5, and Kap 8 of the ca. 2.26 Ga swarm; and Pip 9 of the ca. 1.76 Ga swarm (Fig. 4). Most dyke samples of the ca. 2.80 Ga, ca. 2.76 Ga, ca. 2.26 Ga swarms, and a few of the ca. 1.76 Ga swarm display small negative Eu anomalies, whereas Kes 8 (of the ca. 2.80 Ga swarm) and Kap 3 (of the ca. 2.26 Ga swarm) show slight positive Eu anomalies. The Primitive-Mantle normalized multi-element patterns (Figs. 4e-h) of most of the dykes are characterized by elevated Cs, Rb, U, Th, K, and Pb and troughs of Ba, Nb, Ta, P, and Ti. However, most of the samples from the ca. 1.76 Ga swarm and a few from other swarms do not exhibit negative Ti anomaly. Two features of the multi-element patterns are noteworthy: (1) the dykes are relatively depleted in high field strength elements (HFSE) like Nb, Ta, and Ti, and (2) they show enrichment in LREE, U, Th, and large ion lithophile elements (LILE) like Cs, Rb, K, and Pb.

4.2. Whole-rock Sr and Nd isotopes

The whole-rock Sr and Nd isotope data for the mafic dyke samples are listed in Table 3 and illustrated in Figure 5. Additional Sr and Nd isotope data for dykes of the ca. 2.80 Ga Keshargaria swarm have been taken from Roy et al. (2004) and are listed in Table 3. The calculated initial $^{87}Sr/^{86}Sr$ values ($^{87}Sr/^{86}Sr_i$) for samples from different dyke swarms are: $^{87}Sr/^{86}Sr_{2.80\ Ga} = 0.70014 - 0.70570$, $^{87}Sr/^{86}Sr_{2.76\ Ga} = 0.70412 - 0.70481$, $^{87}Sr/^{86}Sr_{2.26\ Ga} = 0.70326 - 0.70691$, and $^{87}Sr/^{86}Sr_{1.76\ Ga} = 0.70818 - 0.71280$. All samples of the ca. 2.76 Ga, ca. 2.26 Ga, and ca. 1.76 Ga swarms have a $^{87}Sr/^{86}Sr_i$ composition that plot between the growth curves for undifferentiated mantle or the Chondritic Uniform Reservoir (CHUR) and the 3.5 Ga upper continental crust (Rudnick and Gao, 2003) representative of the Singhbhum Craton (Fig. 5a). The samples of the ca. 2.80 Ga swarm exhibit $^{87}Sr/^{86}Sr_i$ compositions that indicate a depleted source for most samples, whereas one sample shows derivation from an enriched source, which support a heterogeneous source for the mafic melts. In general, there is a negative correlation between the $^{87}Sr/^{86}Sr_i$ and age, with younger dykes having more radiogenic initial isotope compositions.

Considerable variability is also observed in the initial ε_{Nd} ($\varepsilon_{Nd(i)}$) of all dyke swarms, which are sub-chondritic for all samples of the ca. 2.76 Ga, ca. 2.26 Ga, and ca. 1.76 Ga swarms; $\varepsilon_{Nd(i)}$ of the ca. 2.80 Ga swarm samples span from super-chondritic to sub-chondritic compositions (Fig. 5b). The $\varepsilon_{Nd(i)}$ of most samples of the four swarms plot between the CHUR-line and the growth array defined by the Paleoarchean granitoid crust of the Singhbhum Craton (Pandey et al., 2019). The Nd isotope compositions ($\varepsilon_{Nd(2.80\ Ga)} = +3.7$ to -1.5; $\varepsilon_{Nd(2.76\ Ga)} = -2.4$ to -2.6; $\varepsilon_{Nd(2.26\ Ga)} = -3.7$ to -7.3; and $\varepsilon_{Nd(1.76\ Ga)} = -5$ to -10) also display a secular trend with the older dykes having higher $\varepsilon_{Nd(i)}$ values and the younger ones having lower (i.e., more negative) values, consistent with the trend observed for the $^{87}Sr/^{86}Sr_i$ isotopic compositions.

5. Discussion

5.1. Petrogenetic constraints from major- and trace-element geochemistry

The Singhbhum Craton dyke swarms exhibit chemical and isotopic heterogeneity within a swarm and among the different dyke swarms

Table 1
Details of the samples from mafic dykes of the Singhbhum Craton.

Sample No.	Latitude (N)	Longitude (E)	Analysis
Keshargaria swarm (NNE-SSW, Emplacement age = 2800[(1)] Ma)			
Om 33	22° 30.174′	85° 52.068′	Whole-rock major & trace, Rb-Sr & Sm-Nd
Kes 2	22° 34.980′	85° 54.572′	Whole-rock major & trace
Kes 3	22° 33.287′	85° 51.113′	Whole-rock major & trace
Kes 4	22° 32.772′	85° 49.337′	Whole-rock major & trace
Kes 5	22° 31.240′	85° 52.388′	Whole-rock major & trace
Kes 6	22° 21.905′	85° 47.293′	Whole-rock major & trace
Kes 7	22° 23.257′	85° 47.342′	Whole-rock major & trace
Kes 8	22° 28.958′	85° 53.898′	Whole-rock major & trace
Ghatgaon swarm (NNE-SSW, Emplacement age = 2762[(1)] Ma)			
Om 23	21° 45.511′	85° 34.426′	Whole-rock major & trace, Rb-Sr & Sm-Nd
OPP 7	21° 45.511′	85° 34.426′	Whole-rock major & trace, Rb-Sr & Sm-Nd
Om 26	22° 00.316′	85° 39.658′	Whole-rock major & trace, Rb-Sr & Sm-Nd
Gha 4	22° 18.453′	85° 59.618′	Whole-rock major & trace
Gha 5	22° 17.058′	85° 49.422′	Whole-rock major & trace
Gha 6	22° 06.770′	85° 51.410′	Whole-rock major & trace
Gha 7	21° 19.025′	85° 48.998′	Whole-rock major & trace
Gha 8	21° 16.213′	85° 53.088′	Whole-rock major & trace
Gha 9	21° 49.995′	85° 50.865′	Whole-rock major & trace
Gha 10	21° 43.498′	85° 43.317′	Whole-rock major & trace
Gha 11	22° 01.708′	85° 59.803′	Whole-rock major & trace
Kaptipada swarm (ENE-WSW, Emplacement age = 2256[(2)] Ma)			
Om 5a	22° 09.770′	86° 14.338′	Whole-rock major & trace, Rb-Sr & Sm-Nd
OPP 2	22° 12.850′	86° 15.120′	Whole-rock major & trace, Rb-Sr & Sm-Nd
Kap 3	22° 28.933′	85° 53.933′	Whole-rock major & trace
Kap 4	22° 26.003′	85° 49.067′	Whole-rock major & trace
Kap 5	22° 12.250′	86° 15.830′	Whole-rock major & trace
Kap 6	21° 20.362′	86° 02.337′	Whole-rock major & trace
Kap 7	21° 29.748′	86° 34′	Whole-rock major & trace
Kap 8	21° 30.327′	86° 32.832′	Whole-rock major & trace
Kap 9	21° 14.832′	86° 04.113′	Whole-rock major & trace
Pipilia swarm (WNW-ESE, Emplacement age = 1765[(3)] Ma)			
Om 13	21° 27.971′	86° 09.572′	Whole-rock major & trace, Rb-Sr & Sm-Nd
Om 14	21° 26.256′	86° 09.879′	Whole-rock major & trace, Rb-Sr & Sm-Nd
Om 19	21° 34.453′	85° 46.341′	Whole-rock major & trace, Rb-Sr & Sm-Nd
OPP 5	21° 34.453′	85° 46.341′	Whole-rock major & trace
Pip 5	21° 41.232′	85° 41.050′	Whole-rock major & trace
Pip 6	21° 31.410′	85° 52.067′	Whole-rock major & trace
Pip 7	21° 34.920′	85° 54.508′	Whole-rock major & trace
Pip 8	21° 23.418′	86° 09.122′	Whole-rock major & trace
Pip 9	21° 28.762′	85° 49.972′	Whole-rock major & trace
Pip 10	21° 21.980′	85° 48.168′	Whole-rock major & trace
Pip 11	22° 01.587′	85° 59.640′	Whole-rock major & trace
Pip 12	21° 26.185′	86° 07.313′	Whole-rock major & trace

Names of the dyke swarms after Srivastava et al. (2019).
Age references: (1) Kumar et al. (2017), (2) Srivastava et al. (2019), (3) Shankar et al. (2014).

(Figs. 2-5). The presence of normative quartz and the sub-equal contents of normative hypersthene and diopside (Table 2) classify them as quartz-gabbronorite (e.g., Le Maitre et al., 2002). The compatible trace elements (e.g., Ni and Cr) are excellent tracers to distinguish between crustal and mantle sources and to evaluate contamination during the emplacement of the melts in the continental crust (e.g., Sobolev et al., 2007). Mantle-derived non-fractionated magmas have high concentrations (i.e., abundances higher than the average MORB, where Ni = 92 ppm, and Cr = 249 ppm; Gale et al., 2013) of these elements. The most primitive Singhbhum dykes have intriguingly high Ni (as high as 590 ppm), Cr (as high as 1110 ppm), and V (as high as 434 ppm) concentrations (Table 2, Figs. 3j-l), which indicate the involvement of a mantle component in the source of the parental magmas (Frey et al., 1978). However, the overall chondrite normalized REE (e.g., enrichment of LREE; Figs. 4a - d) and Primitive-Mantle normalized multi-element patterns (e.g., depletion of HFSE like Nb, Ta, and Ti, and enrichment of LILE like Cs, Rb, K, and Pb; Figs. 4e - h) of these dykes (including the most primitive dykes with Mg# > 60) are similar to those of the bulk continental crust (BCC). The enriched Cs, Rb, K, and Pb, and the negative Nb, Ta, and Ti anomalies indicate involvement of crustal components with an "arc-like" signatures (Fig. 3p) (Perfit et al., 1980). These geochemical signatures indicate that the Singhbhum dykes could have been derived through (1) subduction related magmatism in an arc-setting, or (2) assimilation of crustal material by parental magmas after emplacement at crustal depths, or (3) SCLM enriched by subduction-driven metasomatism (Fig. 6a; e.g., Goodenough et al., 2002; Paul et al., 2020; Zhao and McCulloch, 1993).

5.1.1. Subduction related magmatism

The geochemical signatures (e.g., negative Nb, and Ta anomalies; Figs. 3p and 4) of the Singhbhum dykes show similarities with arc rocks generated by subduction-related magmatism. However, this interpretation is not tenable for the Singhbhum dykes for several reasons: (1) The dykes were emplaced throughout the craton after its cratonization (at ca. 3 Ga) and it is difficult to conceive of a geodynamic scenario involving a subduction zone in the middle of a cratonized lithospsphere. (2) The dykes were emplaced in multiple and discrete magmatic episodes between ca. 2.80 Ga and ca. 1.76 Ga, and subduction

Table 2
Major (wt.%) and trace (ppm) element, and normative mineral (vol.%) composition of mafic dykes of the Singhbhum Craton.

	NNE-trending Keshargaria swarm (ca. 2.80 Ga)								NNE-trending Ghatgaon swarm (ca. 2.76 Ga)										
Analyte	Om 33	Kes 2	Kes 3	Kes 4	Kes 5	Kes 6	Kes 7	Kes 8	Om 23	OPP 7	Om 26	Gha 4	Gha 5	Gha 6	Gha 7	Gha 8	Gha 9	Gha 10	Gha 11
SiO_2	56.58	55.27	50.69	50.92	58.71	52.98	55.58	47.44	52.01	52.40	53.96	56.07	50.67	57.46	54.84	54.28	53.85	49.19	49.40
TiO_2	0.53	0.46	1.25	1.31	0.51	0.30	0.51	1.15	0.24	0.21	1.33	0.69	1.10	1.11	0.66	0.76	1.38	2.00	1.15
Al_2O_3	15.08	12.39	13.67	13.51	14.61	12.01	13.21	15.76	14.81	13.70	10.89	13.76	14.11	12.84	13.53	11.69	13.04	12.80	13.36
$FeO_{(T)}$	8.27	8.19	9.65	10.01	8.46	7.29	8.04	10.55	6.47	6.58	11.48	9.09	13.14	9.78	8.85	9.68	12.04	13.43	13.34
MnO	0.14	0.14	0.16	0.16	0.13	0.14	0.13	0.15	0.13	0.14	0.18	0.15	0.20	0.15	0.15	0.16	0.17	0.19	0.20
MgO	3.89	7.51	7.55	7.77	3.58	10.60	5.83	7.79	9.23	10.10	7.14	5.27	5.17	4.30	5.21	9.99	5.03	5.01	5.90
CaO	7.82	9.84	9.96	9.70	7.24	11.07	7.57	10.64	12.38	11.76	7.09	8.72	8.78	7.22	8.92	8.66	8.90	9.26	10.00
Na_2O	2.96	2.02	1.86	1.84	2.89	1.25	2.46	1.63	1.24	1.48	2.78	2.46	2.71	2.74	2.39	1.81	2.48	2.31	2.22
K_2O	1.72	1.16	1.21	1.33	1.57	0.83	1.87	0.48	0.60	0.46	1.75	1.00	0.67	1.48	1.03	0.65	0.81	0.91	0.27
P_2O_5	0.06	0.08	0.27	0.35	0.09	0.04	0.05	0.10	0.02	0.02	0.14	0.11	0.16	0.38	0.10	0.13	0.17	0.38	0.12
LOI	1.82	2.33	2.69	2.76	1.96	3.46	2.68	3.78	2.90	2.74	1.78	2.34	2.45	1.57	1.98	1.77	1.29	2.31	2.10
Total	98.87	99.39	98.96	99.66	99.75	99.97	97.93	99.47	100.0	99.58	98.52	99.66	99.15	99.03	97.65	99.58	99.16	97.78	98.05
Mg#	46	62	58	58	43	72	56	57	72	73	53	51	41	44	51	65	43	40	44
Sc	24	33	31	30	24	32	27	26	31	31	22	29	34	26	28	29	30	32	36
V	155	172	241	225	165	152	170	243	128	120	181	204	199	181	202	214	329	338	273
Cr	50	500	400	370	40	770	300	210	310	350	560	140	130	130	140	720	150	120	160
Ni	60	170	120	150	40	310	140	230	420	280	420	110	80	70	100	200	70	70	110
Cu	70	70	90	90	50	90	70	110	90	40	280	80	80	70	80	70	140	110	110
Zn	80	70	80	80	80	60	70	70	40	40	90	80	90	100	80	80	90	130	100
Rb	80	51	45	64	62	30	71	21	25	19	59	30	33	52	33	31	23	41	9
Sr	229	149	209	225	199	133	184	206	116	78	371	200	181	216	190	135	206	179	166
Y	25.4	25.0	23.9	29.4	26.5	14.0	22.4	16.0	15.9	14.8	21.5	20.7	30.7	41.9	19.7	18.6	21.2	49.3	24.2
Zr	132	121	146	203	146	59	105	67	62	49	131	107	94	257	103	77	93	258	77
Nb	9.6	8.2	6.1	8.7	8.6	3.5	6.5	2.8	4.4	4.1	11.6	4.6	3.8	10.5	4.3	3.4	4.3	15.6	3.0
Cs	1.1	0.9	0.8	1.0	0.6	0.4	0.6	1.7	0.8	0.4	0.8	1.7	2.9	4.0	0.5	4.2	0.9	3.9	1.5
Ba	263	166	178	208	244	105	269	74	106	89	389	316	139	443	285	181	175	211	59
La	26.5	24.4	14.6	19.6	28.8	11.3	22.4	5.4	12.2	9.8	23.7	18.3	6.2	32.8	17.6	11.6	13.6	32.7	6.8
Ce	50.7	47.0	30.9	41.1	54.7	21.9	42.0	12.8	23.7	18.7	49.1	36.2	15.8	68.2	34.6	24.2	28.2	67.1	15.9
Pr	5.42	5.14	3.77	4.98	5.93	2.36	4.51	1.81	2.60	2.12	6.05	4.15	2.32	8.20	3.96	2.86	3.34	7.95	2.13
Nd	19.6	17.9	15.6	20.2	20.8	9.0	16.0	8.4	9.6	7.9	24.6	16.0	11.2	32.3	15.4	11.8	14.1	31.6	9.7
Sm	4.00	3.81	3.76	4.50	4.22	2.03	3.36	2.37	2.08	1.85	5.32	3.55	3.49	7.31	3.44	2.82	3.38	7.47	2.93
Eu	0.99	0.84	1.21	1.34	1.01	0.55	0.79	1.03	0.57	0.49	1.46	0.95	1.22	1.94	0.99	0.89	1.22	2.07	1.07
Gd	4.02	3.94	4.11	4.90	4.08	2.12	3.50	2.94	2.27	1.98	4.88	3.70	4.60	7.30	3.56	3.13	3.78	8.16	3.64
Tb	0.68	0.67	0.72	0.87	0.73	0.39	0.63	0.49	0.41	0.36	0.73	0.64	0.86	1.30	0.59	0.54	0.66	1.44	0.67
Dy	4.37	4.17	4.28	5.01	4.45	2.42	3.88	3.01	2.56	2.42	4.07	3.58	5.36	7.52	3.51	3.39	3.93	8.65	4.16
Ho	0.93	0.90	0.87	1.04	0.91	0.50	0.80	0.61	0.54	0.51	0.75	0.76	1.14	1.50	0.69	0.67	0.80	1.78	0.88
Er	2.79	2.62	2.44	3.01	2.74	1.51	2.34	1.76	1.61	1.58	2.02	2.23	3.31	4.45	2.04	1.97	2.17	5.22	2.67
Tm	0.410	0.389	0.351	0.431	0.402	0.225	0.350	0.254	0.247	0.234	0.282	0.324	0.503	0.655	0.303	0.291	0.326	0.755	0.404
Yb	2.66	2.59	2.28	2.80	2.76	1.43	2.34	1.58	1.67	1.55	1.76	2.08	3.40	4.31	2.04	1.90	2.08	4.87	2.69
Lu	0.406	0.400	0.380	0.441	0.434	0.226	0.359	0.249	0.256	0.243	0.252	0.332	0.549	0.680	0.295	0.291	0.310	0.788	0.419
Hf	3.5	3.0	3.2	4.2	3.8	1.5	2.8	1.8	1.6	1.2	3.4	2.8	2.6	6.1	2.7	1.9	2.5	6.3	2.1
Ta	0.74	0.64	0.43	0.61	0.73	0.27	0.62	0.20	0.15	0.24	0.28	0.36	0.25	0.80	0.43	0.28	0.35	0.99	0.20
Pb	10	8	< 5	< 5	11	< 5	10	< 5	<5	<5	7	7	< 5	11	7	< 5	< 5	7	< 5

Th	6.66	5.79	2.16	3.13	7.35	2.60	6.08	0.47	2.67	2.00	4.15	3.73	0.80	6.59	3.49	2.37	2.59	5.81	0.77
U	1.63	1.44	0.52	0.74	1.74	0.62	1.62	0.11	0.62	0.49	1.01	0.92	0.19	1.70	0.84	0.65	0.60	1.25	0.17
Th/Yb	2.50	2.24	0.95	1.12	2.66	1.82	2.60	0.30	1.60	1.29	2.36	1.79	0.24	1.53	1.71	1.25	1.25	1.19	0.29
Nb/Yb	3.61	3.17	2.68	3.11	3.12	2.45	2.78	1.77	2.61	2.63	6.57	2.21	1.12	2.44	2.11	1.79	2.07	3.20	1.12
Eu/Eu*	0.76	0.66	0.94	0.87	0.74	0.81	0.70	1.19	0.80	0.77	0.88	0.80	0.93	0.81	0.86	0.91	1.04	0.81	1.00
$(La/Lu)_N$	7.00	6.54	4.12	4.76	7.11	5.36	6.69	2.32	5.11	4.31	10.08	5.91	1.20	5.17	6.39	4.27	4.70	4.45	1.74
quartz	9.1	8.4	2.5	2.3	13.7	5.4	8.9	0.0	4.4	4.0	3.6	11.0	1.8	13.6	10.3	7.1	8.2	2.9	2.1
plagioclase	53.1	43.7	47.6	46.4	51.3	40.6	46.0	56.1	49.2	47.9	41.6	49.9	55.2	46.6	49.6	42.7	49.2	49.4	52.8
orthoclase	11.8	8.2	8.8	9.6	10.7	6.0	13.2	3.5	4.3	3.3	12.6	7.0	4.8	10.3	7.4	4.6	5.8	6.7	2.0
diopside	11.6	20.3	17.2	16.2	9.6	22.9	13.4	14.0	21.2	21.8	17.2	14.3	14.1	11.2	15.6	15.4	16.0	17.1	18.4
hypersthene	12.8	17.9	20.8	22.0	13.1	23.8	16.9	21.4	19.9	22.1	21.9	15.9	21.1	15.2	15.3	27.9	17.6	19.1	21.7
olivine	0	0	0	0	0	0	0	2.27	0	0	0	0	0	0	0	0	0	0	0
ilmenite	0.64	0.56	1.57	1.63	0.6	0.37	0.62	1.46	0.3	0.25	1.67	0.84	1.37	1.33	0.81	0.95	1.7	2.56	1.46
magnetite	0.77	0.78	0.93	0.97	0.77	0.71	0.77	1.03	0.62	0.63	1.11	0.85	1.28	0.91	0.85	0.93	1.15	1.33	1.32
apatite	0.13	0.17	0.61	0.79	0.19	0.09	0.11	0.22	0.04	0.04	0.31	0.23	0.37	0.83	0.21	0.29	0.37	0.89	0.27
zircon	0.02	0.02	0.02	0.03	0.02	0.01	0.01	0.01	0.01	0.01	0.02	0.01	0.01	0.03	0.01	0.01	0.01	0.03	0.01
chromite	0.01	0.06	0.05	0.04	0.01	0.1	0.03	0.03	0.04	0.04	0.07	0.02	0.02	0.02	0.02	0.1	0.02	0.02	0.02
Total	100	100	99.99	99.99	100.01	100	100.01	99.99	100	99.99	100	100	99.99	100.01	100	100.01	100	100	100

	ENE-trending Kaptipada swarm (ca. 2.26 Ga)									WNW -trending Pipilia swarm (ca. 1.76 Ga)											
Analyte	Om 5a	OPP 2	Kap 3	Kap 4	Kap 5	Kap 6	Kap 7	Kap 8	Kap 9	Om13	Om 14	Om 19	OPP 5	Pip 5	Pip 6	Pip 7	Pip 8	Pip 9	Pip 10	Pip 11	Pip 12
SiO_2	56.87	54.08	53.65	57.92	49.68	52.26	54.90	51.13	49.35	50.80	52.44	58.72	58.88	51.74	60.02	59.81	53.03	50.51	54.18	49.40	50.69
TiO_2	0.51	0.57	0.71	0.56	1.25	0.79	0.53	0.97	2.47	1.75	1.22	1.20	1.17	1.58	1.22	1.21	1.86	0.23	0.98	1.43	1.88
Al_2O_3	14.27	12.65	11.76	13.43	12.86	13.31	12.36	13.31	13.36	13.04	10.81	11.81	12.43	12.98	12.30	11.81	12.58	10.20	9.95	9.97	11.31
$FeO_{(T)}$	8.44	9.25	9.06	7.61	12.89	10.48	8.93	11.31	13.03	11.97	10.82	8.94	8.94	10.97	8.82	8.86	12.07	8.21	11.22	11.61	12.93
MnO	0.30	0.16	0.15	0.13	0.20	0.18	0.15	0.19	0.22	0.15	0.19	0.12	0.13	0.16	0.12	0.12	0.16	0.15	0.16	0.16	0.18
MgO	5.94	9.53	10.71	5.39	5.87	6.53	8.46	7.18	4.50	5.53	8.34	4.69	5.13	6.93	4.79	4.78	5.03	16.80	10.17	10.80	7.53
CaO	7.95	7.87	8.57	6.60	10.78	10.54	7.33	10.14	9.11	7.42	10.09	6.04	6.30	8.20	5.91	5.96	7.34	8.13	7.53	7.18	8.55
Na_2O	2.57	1.57	1.74	2.46	1.74	1.97	1.59	1.90	2.23	2.90	2.35	3.01	3.20	2.75	3.13	3.05	3.13	1.04	1.62	1.74	2.67
K_2O	1.15	1.27	0.94	2.16	0.24	0.78	1.25	1.22	1.84	1.47	0.81	1.63	1.62	1.34	1.69	1.65	1.29	0.85	1.25	1.06	0.90
P_2O_5	0.08	0.08	0.02	0.09	0.12	0.12	0.09	0.11	0.53	0.14	0.11	0.13	0.12	0.18	0.15	0.16	0.19	0.03	0.12	0.16	0.19
LOI	1.22	2.50	2.21	2.56	2.40	2.37	3.25	1.94	2.50	2.02	1.38	1.41	1.48	2.28	1.46	1.64	1.71	3.38	2.02	3.49	2.18
Total	99.30	99.53	99.52	98.91	98.03	99.33	98.84	99.39	99.13	97.19	98.55	97.69	99.40	99.11	99.61	99.06	98.38	99.52	99.20	97.00	99.01
Mg#	56	65	68	56	45	53	63	53	38	45	58	48	51	53	49	49	43	78	62	62	51
Sc	25	29	27	24	45	42	28	43	38	23	30	17	18	27	17	17	20	25	23	21	30
V	154	188	188	167	301	242	180	266	294	354	252	210	207	322	218	219	374	130	203	250	434
Cr	220	640	1110	240	100	100	560	220	100	180	340	270	290	380	290	300	170	2150	1040	700	410
Ni	260	190	340	120	70	70	160	80	< 20	220	310	210	160	200	140	140	140	730	360	590	230
Cu	100	80	80	60	160	90	70	80	40	180	190	100	90	120	80	80	180	30	140	130	160
Zn	70	60	70	70	90	80	70	90	120	100	80	80	100	70	80	80	110	70	80	100	100
Rb	40	68	34	92	13	37	64	69	58	55	29	50	53	48	49	49	62	41	63	56	31
Sr	236	113	141	118	136	193	111	170	290	229	235	252	289	268	284	269	246	140	177	221	225
Y	19.3	17.3	10.1	25.9	25.2	18.4	17.0	20.0	35.7	23.9	20.5	20.6	23.4	21.6	17.9	18.7	25.2	8.7	19.6	21.9	23.7
Zr	96	87	31	140	70	66	86	66	197	133	107	129	178	129	135	140	162	40	126	122	146
Nb	5.6	6.7	1.7	8.9	3.4	5.8	4.6	5.6	26	7.9	6.1	7.2	7.1	5.6	5.9	6.3	7.0	1.4	6.7	5.2	6.0
Cs	2.9	5.0	1.5	0.7	0.6	1.5	3.1	0.6	1.3	0.8	2.3	1.4	1.4	1.3	1.5	1.5	1.6	5.5	4.0	5.8	1.5
Ba	349	224	147	308	43	180	216	155	667	296	182	279	279	270	259	253	227	135	245	159	177

(continued on next page)

Table 2 (*continued*)

	ENE-trending Kaptipada swarm (ca. 2.26 Ga)									WNW -trending Pipilia swarm (ca. 1.76 Ga)											
Analyte	Om 5a	OPP 2	Kap 3	Kap 4	Kap 5	Kap 6	Kap 7	Kap 8	Kap 9	Om13	Om 14	Om 19	OPP 5	Pip 5	Pip 6	Pip 7	Pip 8	Pip 9	Pip 10	Pip 11	Pip 12
La	18.5	14.9	4.8	27.1	6.3	11.5	17.9	8.4	42.5	16.6	14.0	21.5	23.5	15.4	21.3	22.0	20.9	7.5	21.9	15.5	17.4
Ce	37.8	29.6	9.6	51.2	14.8	23.6	33.9	18.2	85.4	35.2	30.0	42.3	45.3	33.4	41.9	42.9	43.6	14.0	43.8	33.0	37.2
Pr	4.13	3.21	1.12	5.48	2.02	2.74	3.68	2.22	9.89	4.39	3.81	4.89	5.15	4.13	4.67	4.85	5.35	1.52	5.05	4.06	4.70
Nd	15.7	12.3	4.7	19.8	9.3	11.2	13.4	10.0	39.6	18.8	16.1	19.0	20.5	18.0	18.0	19.0	22.4	5.7	19.9	17.0	20.2
Sm	3.39	2.75	1.21	4.05	2.78	2.67	2.80	2.72	8.04	4.94	4.44	4.42	4.43	4.53	4.07	4.34	5.64	1.21	4.53	4.48	5.23
Eu	0.98	0.74	0.54	0.86	1.07	0.95	0.72	0.96	2.72	1.65	1.38	1.44	1.46	1.46	1.32	1.30	1.87	0.37	1.19	1.45	1.68
Gd	3.27	2.80	1.53	4.05	3.70	3.05	2.79	3.14	7.65	5.00	4.28	4.34	4.96	4.89	4.10	4.15	5.77	1.14	4.17	4.89	5.23
Tb	0.54	0.46	0.29	0.71	0.73	0.54	0.51	0.58	1.22	0.80	0.68	0.68	0.81	0.82	0.66	0.67	0.91	0.21	0.69	0.80	0.84
Dy	3.33	2.88	1.74	4.23	4.29	3.20	2.93	3.58	6.74	4.65	3.92	3.80	4.62	4.35	3.63	3.71	5.14	1.44	3.76	4.39	4.84
Ho	0.69	0.60	0.36	0.89	0.92	0.67	0.58	0.72	1.34	0.84	0.76	0.68	0.88	0.80	0.67	0.69	0.94	0.31	0.72	0.80	0.89
Er	1.92	1.81	1.08	2.67	2.74	1.91	1.77	2.19	3.78	2.29	2.00	1.81	2.33	2.14	1.78	1.80	2.48	0.97	2.07	2.15	2.45
Tm	0.290	0.274	0.158	0.391	0.398	0.280	0.263	0.302	0.522	0.310	0.274	0.257	0.320	0.299	0.234	0.248	0.330	0.149	0.285	0.297	0.319
Yb	1.89	1.75	1.13	2.58	2.56	1.91	1.77	2.03	3.43	1.89	1.80	1.63	1.85	1.74	1.46	1.46	1.97	0.99	1.77	1.78	1.96
Lu	0.288	0.267	0.178	0.401	0.383	0.285	0.289	0.336	0.551	0.280	0.254	0.243	0.271	0.268	0.207	0.211	0.296	0.161	0.264	0.253	0.285
Hf	2.4	2.0	0.9	3.4	1.9	1.8	2.3	1.9	4.7	3.5	2.7	3.4	3.5	3.6	3.4	3.7	4.3	1.0	3.3	3.3	3.9
Ta	0.11	0.26	0.20	0.74	0.25	0.39	0.55	0.43	1.51	0.27	0.19	0.40	0.55	0.43	0.46	0.47	0.56	0.09	0.60	0.40	0.47
Pb	9	11	< 5	11	< 5	< 5	12	< 5	< 5	6	<5	8	12	7	9	9	9	< 5	12	< 5	8
Th	4.13	5.46	1.06	7.55	1.05	2.08	6.76	1.28	3.52	3.71	2.61	4.78	4.50	3.00	4.82	4.93	4.87	1.18	7.12	3.04	3.37
U	1.09	2.03	0.31	1.91	0.26	0.40	2.39	0.26	0.51	0.93	0.61	1.19	1.23	0.75	1.19	1.30	1.17	0.19	2.23	0.73	0.82
Th/Yb	2.19	3.12	0.94	2.93	0.41	1.09	3.82	0.63	1.03	1.96	1.45	2.93	2.43	1.72	3.30	3.38	2.47	1.19	4.02	1.71	1.72
Nb/Yb	2.95	3.81	1.50	3.45	1.33	3.04	2.60	2.76	7.46	4.18	3.40	4.43	3.83	3.22	4.04	4.32	3.55	1.41	3.79	2.92	3.06
Eu/Eu*	0.90	0.81	1.22	0.65	1.02	1.02	0.79	1.01	1.06	1.01	0.97	1.01	0.95	0.95	0.99	0.94	1.00	0.96	0.84	0.95	0.98
$(La/Lu)_N$	6.88	5.98	2.88	7.24	1.77	4.32	6.64	2.66	8.27	6.35	5.91	9.48	9.29	6.16	11.03	11.17	7.57	4.96	8.89	6.57	6.54
quartz	10.3	7.2	4.9	12.6	5.3	5.2	11.1	1.5	1.7	1.2	2.4	15.0	12.4	1.0	15.0	15.7	4.6	0.0	7.2	1.0	0.2
plagioclase	50.8	42.2	41.7	44.7	49.1	48.2	41.8	46.5	46.5	50.5	42.8	44.6	46.7	49.2	45.5	44.2	49.9	34.8	34.9	38.1	46.1
orthoclase	7.9	9.1	6.7	15.0	1.8	5.6	9.0	8.8	13.3	10.7	5.9	11.4	11.1	9.6	11.5	11.4	9.2	6.3	9.0	8.1	6.6
diopside	11.1	11.3	16.0	9.6	20.7	20.2	9.9	19.5	16.2	13.9	25.4	11.4	11.6	15.7	10.2	11.0	14.4	15.3	15.8	14.9	19.6
hypersthene	18.4	28.4	28.8	16.6	19.9	18.5	26.4	21.2	16.6	20.0	20.6	15.0	15.7	21.1	15.2	15.0	18.0	35.7	30.3	34.3	23.4
olivine	0	0	0	0	0	0	0	0	0	0	0	0	0	0	0	0	0	6.46	0	0	0
ilmenite	0.6	0.71	0.88	0.67	1.61	0.98	0.66	1.2	3.1	2.21	1.54	1.45	1.39	1.97	1.44	1.44	2.31	0.28	1.24	1.9	2.39
magnetite	0.78	0.89	0.87	0.71	1.29	1.01	0.86	1.09	1.27	1.18	1.06	0.84	0.82	1.06	0.81	0.82	1.16	0.82	1.09	1.19	1.27
apatite	0.17	0.17	0.04	0.19	0.29	0.26	0.19	0.24	1.21	0.33	0.24	0.27	0.25	0.41	0.32	0.34	0.44	0.07	0.27	0.38	0.45
zircon	0.01	0.01	0	0.02	0.01	0.01	0.01	0.01	0.03	0.02	0.01	0.02	0.02	0.02	0.02	0.02	0.02	0.01	0.02	0.02	0.02
chromite	0.03	0.08	0.14	0.03	0.01	0.01	0.07	0.03	0.01	0.03	0.04	0.03	0.03	0.05	0.03	0.03	0.02	0.28	0.13	0.09	0.05
Total	100	100	99.99	100.01	99.99	100	99.99	100	99.99	100	99.99	99.99	100	100	100	100	100.01	100	100	100	99.99

LOI = loss on ignition; Mg# = (Mg/Mg+Fe) x 100 (molar); $Eu/Eu^* = (Eu)_N/\{(Sm)_N x (Gd)_N\}^{1/2}$; $(Eu)_N$, $(Sm)_N$, $(Gd)_N$, and $(La/Lu)_N$ are normalized to chondrite (Sun and McDonough, 1989).

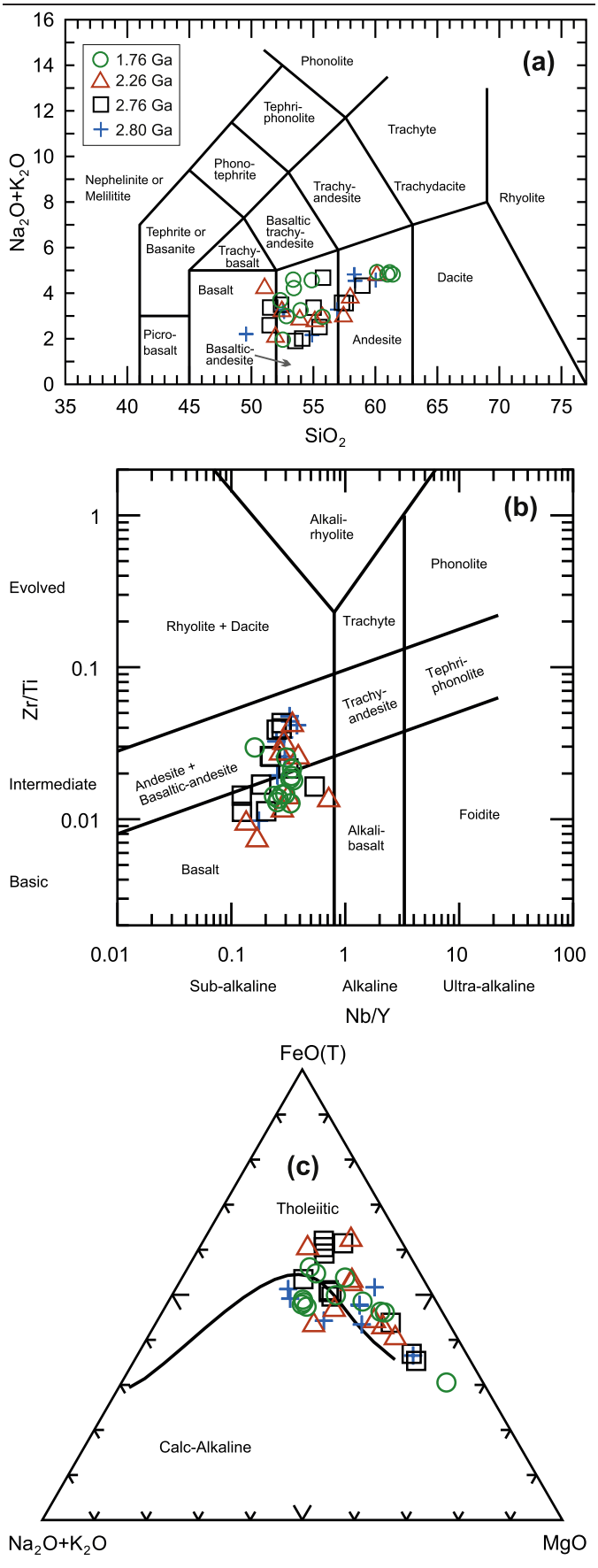

is unlikely to have operated over a period of ~1 Gyr in the same place. (3) If several events of subduction operated at different times, there should be some field/tectonic evidences of arcs, major crustal sutures, accretionary wedges and related feaures/rocks, but till date no such features have been identified in the Singhbhum Craton. (5) The dykes of each swarm display parallel to sub-parallel intrusion patterns, and were emplaced in short magmatic pulses. Each swarm length extends upto more than 100 km with individual dyke widths from 50 to 500 m. The dykes are more closely spaced towards one end (southern) which is a characteristic feature of LIPs and mantle plume-related magmatism (e.g., Bryan and Ernst, 2008; Ernst, 2014). (6) Apparent arc signatures have been reported from many continental LIPs (e.g., the Karoo LIP in the southern Africa), but have also been observed for some oceanic LIPs (e.g., the Wrangellia LIP in the Pacific) (see Ernst, 2014). Similar observations and interpretations have also been reported for the Jurassic igneous rocks of the Sanandaj–Sirjan zone in Iran (Azizi and Stern, 2019; see also the further discussion in Elahi-Janatmakan et al. (2020) and Azizi and Stern (2020)), and the early Cretaceous intra-plate basalts from the western North China Craton (Zhang et al., 2020). Therefore, it can be concluded that the Singhbhum dyke swarms were not generated in an active continental margin or arc setting.

5.1.2. Crustal assimilation

The trace element patterns (Fig. 4) of most of the samples (including the primitive dykes with Mg# > 60) have strong similarities with those of crustal rocks, i.e., enrichment in incompatible elements, negative HFSE anomalies, and an overall element abundance similar to that of the average continental crust (Rudnick and Gao, 2003). If such patterns were the result of assimilation of crustal material by a depleted basaltic melt (NMORB-like; Sun and McDonough, 1989), addition of ~50-90 % by mass of crustal material is required to reproduce the incompatible element abundances in the dykes. This would have to be an assimilation and fractional crystallization (AFC) process resulting in strong depletion of compatible elements (Ni, Cr, V, etc.), and in a bulk composition that is closer to granodiorite than basalt. However, none of the dykes have felsic composition or contain any visible remnants of partially assimilated crustal material. Besides, it is thermodynamically not possible for a basaltic melt to assimilate 50-90% of felsic material without prior solidification. Chemical and textural features indicative of crustal assimilation are absent in the dykes. The rocks with lower Mg# (< 50) were derived essentially from evolved melts that underwent some fractional crystallization of mafic minerals. This fractionation of a basaltic melt is also evident from the bivariate diagrams (Fig. 3).

During magmatic differentiation, Ni is preferentially incorporated into olivine (in basalt-andesite partition-coefficient K_d(Ni) = 22; Dostal et al., 1983) and into clinopyroxene (in basalt-andesite K_d(Ni) = 4; Dostal et al., 1983), Cr into clinopyroxene (in basalt-andesite K_d (Cr) = 28-40; Dostal et al., 1983) and into spinel (in Lunar basalt K_d (Cr) = 10; Klemme et al., 2006), and V into magnetite (in basalt-andesite K_d(V) = 24-63; Reid, 1983). Thus, fractional crystallization of olivine, clinopyroxene, and magnetite result in strong depletion of Ni, Cr, and V in the differentiating magma. If the parental magma of the dykes had assimilated crustal material (at crustal depths), it would lead to crystallization of these mafic phases leaving the evolved melt poor in Ni, Cr, and V. This is contrary to the high Ni, Cr, and V concentrations observed in the primitive dykes (Mg# > 60). Additionally, the

Fig. 2. Classification diagram for the mafic dykes of the Singhbhum Craton. (a) Total Alkali-Silica diagram (TAS; after Le Maitre et al., 1989). (b) Zr/Ti vs. Nb/Y rock type diagram (after Pearce, 1996). (c) AFM diagram (after Irvine and Baragar, 1971) showing whole-rock major element compositions presented in Table 2. All major-oxide concentrations normalized to 100% on a volatile-free basis.

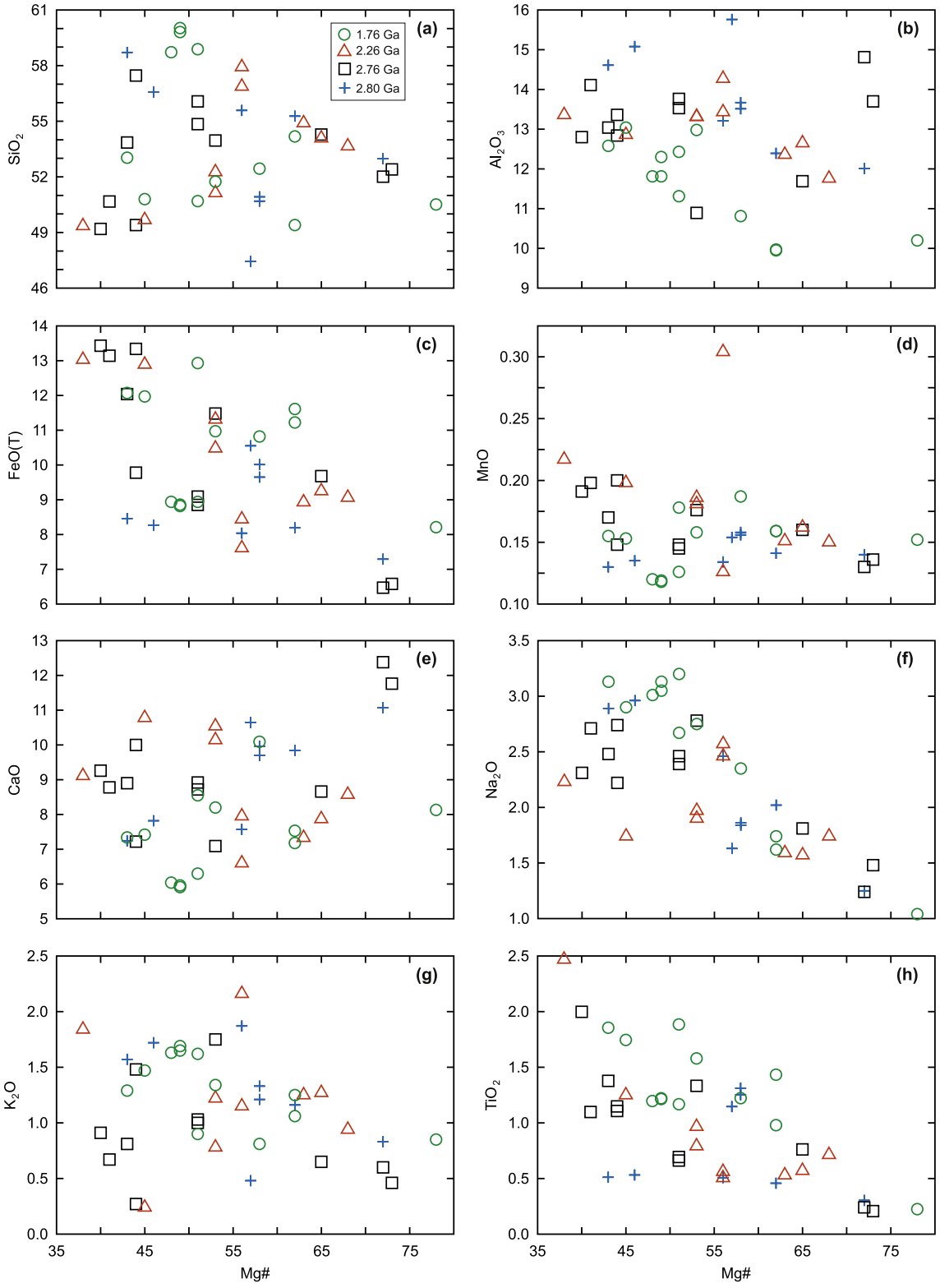

Fig. 3. Major-trace element variation diagrams for whole rock analyses (Table 2). All oxides are in wt.%; V, Ni Cr, and Zr are in ppm. Mg# = (Mg/Mg+Fe) × 100 (molar). $(La/Lu)_N$ is normalized to chondrite (Sun and McDonough, 1989). (o) Th/Yb vs. Nb/Yb diagram after Pearce (2008), the composition of the upper continental crust (UCC) is taken from Rudnick and Gao (2003); (p) Th-Zr-Nb tectonic discrimination diagram after Wood (1980).

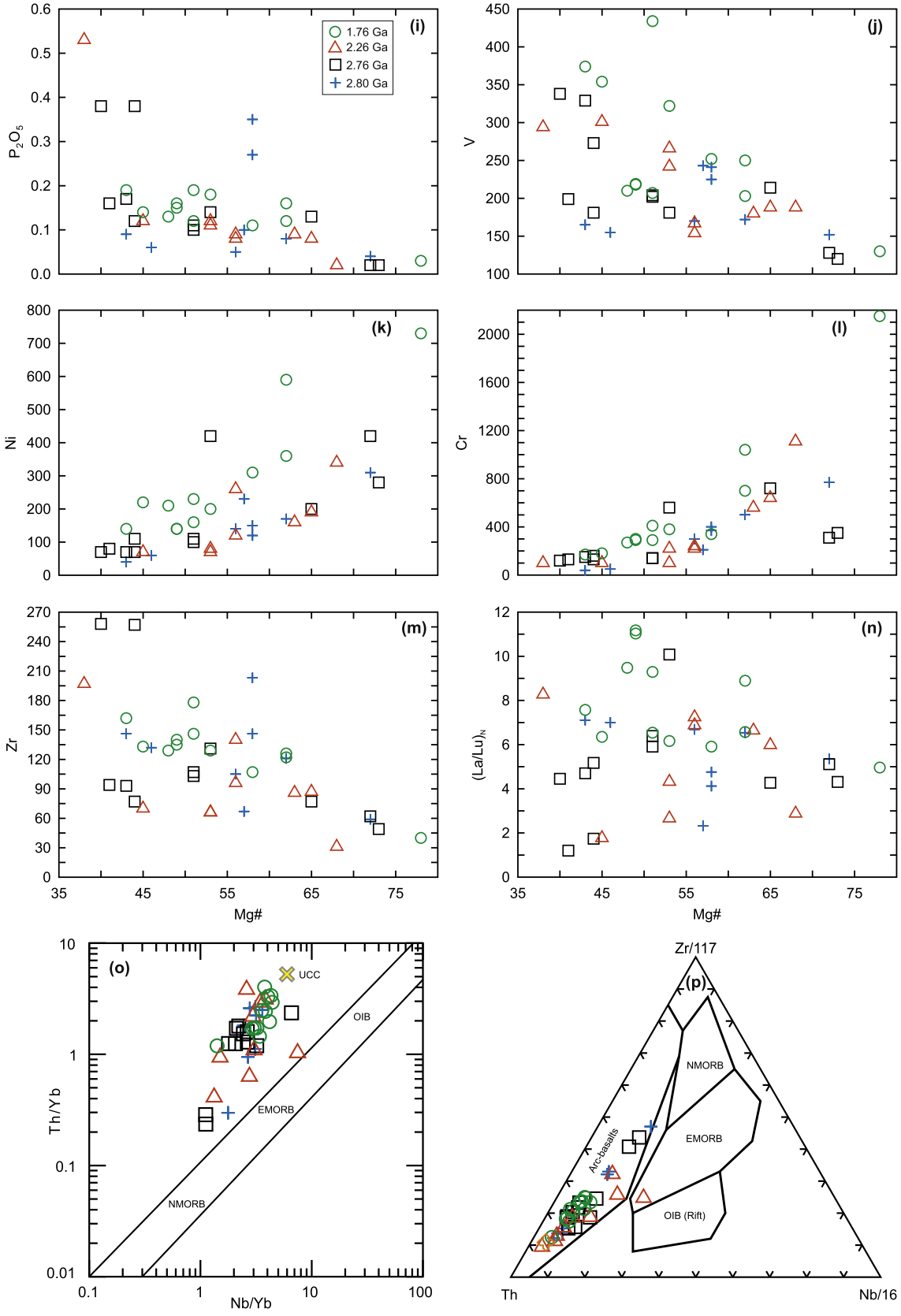

Pandey et al. Fig. 3 (continued)

Fig. 3 (*continued*).

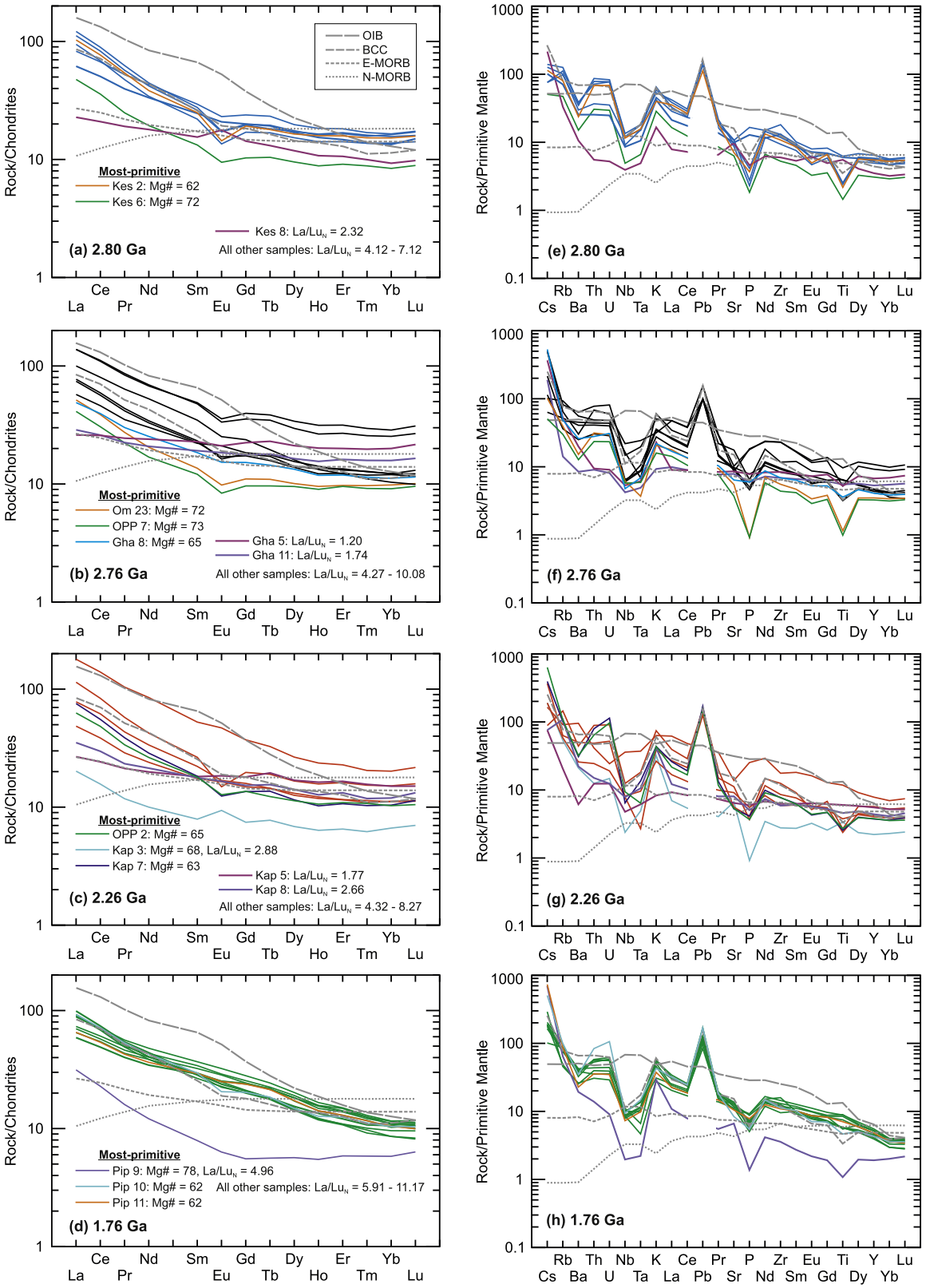

Fig. 4. Chondrite-normalized REE and Primitive-Mantle normalized multi-element plots. For comparison, compositions of the enriched mid-ocean ridge basalt (E-MORB), normal MORB (N-MORB), ocean island basalt (OIB), and bulk continental crust (BCC) are shown. Compositions of the E-MORB, N-MORB, and OIB are after Sun and McDonough (1989), and BCC after Rudnick and Gao (2003).

Table 3
Sr and Nd isotope data for mafic dykes of the Singhbhum Craton.

Sample No.	Age (Ma)	Rb (ppm)	Sr (ppm)	$^{87}Rb/^{86}Sr$	$^{87}Sr/^{86}Sr$	2se	$(^{87}Sr/^{86}Sr)_i$	Sm (ppm)	Nd (ppm)	$^{147}Sm/^{144}Nd$	$^{143}Nd/^{144}Nd$	2se	$(^{143}Nd/^{144}Nd)_i$	ε_{Ndi}
Keshargaria swarm														
Om 33	2800[1]	80.44	228.7	1.015	0.746179	0.000015	0.70570	3.524	18.18	0.1172	0.511121	0.000012	0.508956	-1.0
J 5*	2800[1]	8.490	10.03	2.468	0.792071	0.000016	*0.69360*	0.622	3.718	0.1012	0.511068	0.000010	0.509198	+3.7
J 7*	2800[1]	-	-	-	-	-	-	0.469	2.353	0.1206	0.511261	0.000008	0.509032	+0.48
J 8*	2800[1]	12.87	17.33	2.164	0.783202	0.000018	*0.69686*	0.498	2.975	0.1075	0.511172	0.000009	0.509185	+3.5
J 10*	2800[1]	-	-	-	-	-	-	0.671	3.963	0.1032	0.511091	0.000016	0.509184	+3.5
J 11*	2800[1]	-	-	-	-	-	-	0.572	3.025	0.1142	0.511111	0.000010	0.509000	-0.14
J 12*	2800[1]	10.32	15.47	1.942	0.776752	0.000012	*0.69927*	0.748	4.003	0.1129	0.511162	0.000012	0.509075	+1.3
ND 24*	2800[1]	-	-	-	-	-	-	0.576	2.987	0.1166	0.511190	0.000009	0.509035	+0.54
ND 27*	2800[1]	5.150	8.865	1.690	0.768063	0.000028	0.70063	0.569	2.809	0.1224	0.511228	0.000017	0.508966	-0.82
ND 28*	2800[1]	30.23	163.1	0.5370	0.721410	0.000021	*0.69998*	3.637	15.06	0.1460	0.511812	0.000009	0.509114	+2.1
ND 23*	2800[1]	-	-	-	-	-	-	3.729	17.84	0.1263	0.511267	0.000012	0.508933	-1.5
ND 15*	2800[1]	19.88	30.62	1.890	0.775552	0.000018	0.70014	1.013	5.124	0.1195	0.511209	0.000009	0.509000	-0.14
ND 29*	2800[1]	35.84	128.8	0.8070	0.731941	0.000017	*0.69974*	2.669	13.05	0.1237	0.511308	0.000011	0.509022	+0.28
ND 30*	2800[1]	5.380	11.16	1.401	0.755152	0.000021	*0.69925*	0.625	2.919	0.1292	0.511435	0.000011	0.509047	+0.78
Ghatgaon swarm														
Om 23	2762[1]	25.70	116.8	0.6424	0.729572	0.000019	0.70430	2.308	10.65	0.1310	0.511312	0.000003	0.508925	-2.6
OPP 7	2762[1]	19.18	82.55	0.6737	0.730626	0.000016	0.70412	2.009	8.981	0.1352	0.511399	0.000004	0.508934	-2.4
Om 26	2762[1]	58.68	397.3	0.4279	0.721640	0.000012	0.70481	5.458	25.48	0.1295	0.511283	0.000004	0.508923	-2.6
Kaptipada swarm														
Om 5a	2256[2]	41.27	249.4	0.4793	0.722257	0.000024	0.70691	3.260	15.75	0.1251	0.511203	0.000004	0.509344	-7.3
OPP 2	2256[2]	71.02	114.4	1.805	0.761075	0.000014	0.70326	2.975	13.99	0.1285	0.511438	0.000003	0.509527	-3.7
Pipilia swarm														
Om 13	1765[3]	55.74	241.1	0.6700	0.727467	0.000027	0.71074	4.880	19.46	0.1516	0.511807	0.000003	0.510047	-6.0
Om 14	1765[3]	31.00	253.5	0.3541	0.717025	0.000021	0.70818	4.170	16.75	0.1505	0.511845	0.000004	0.510098	-5.0
Om 19	1765[3]	49.70	273.4	0.5269	0.725753	0.000019	0.71260	4.396	19.65	0.1352	0.511404	0.000003	0.509835	-10
OPP 5	1765[3]	52.77	296.6	0.5156	0.725669	0.000013	0.71280	4.121	18.37	0.1356	0.511415	0.000004	0.509840	-10

Age references: (1) Kumar et al. (2017), (2) Srivastava et al. (2019), (3) Shankar et al. (2014).
*Data from Roy et al. (2004); initial isotopic compositions recalculated.
se = standard error of the mean; i = initial; CHUR = Chondritic Uniform Reservoir; t_0 = present day.
Errors on Rb, Sr concentration and $^{87}Rb/^{86}Sr$ are ~0.5%; on Sm, Nd concentration and $^{147}Sm/^{144}Nd$ are ~0.1%. Maximum uncertainties on $(^{87}Sr/^{86}Sr)_i$ and ε_{Ndi} are ~0.02% and ~1ε, respectively.
Parameters used for initial $^{87}Sr/^{86}Sr$ calculation: $(^{87}Sr/^{86}Sr)_{CHUR}t_0 = 0.7045$; $(^{87}Rb/^{86}Sr)_{CHUR} = 0.0827$; $\lambda_{87Rb} = 1.3972 \times 10^{-11}$ a^{-1} (Villa et al., 2015).
Parameters used for initial $^{143}Nd/^{144}Nd$ and ε_{Ndi} calculation: $(^{143}Nd/^{144}Nd)_{CHUR}t_0 = 0.512630$, $(^{147}Sm/^{144}Nd)_{CHUR} = 0.1960$ (Bouvier et al., 2008); $\lambda_{147Sm} = 6.54 \times 10^{-12}$ a^{-1}.
$(^{87}Sr/^{86}Sr)_i$ data in *italics* are lower than or very close to the solar system initial (~0.699; Papanastassiou and Wasserburg, 1969), therefore, are erroneous and excluded from interpretation.

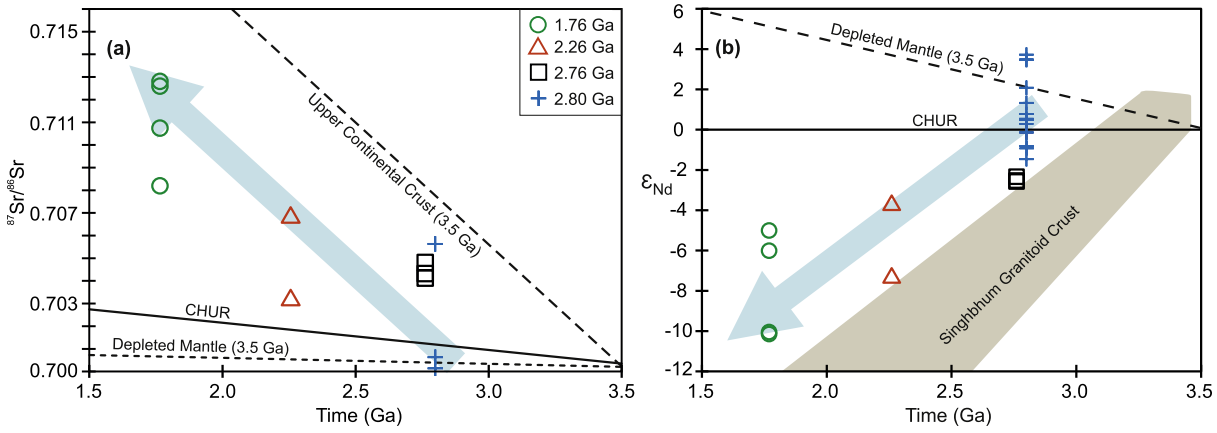

Fig. 5. (a) Whole-rock $^{87}Sr/^{86}Sr$ vs. time (Ga) plot for mafic dykes of the Singhbhum Craton (Table 3). The Sr isotope evolution lines for the 3.5 Ga Upper Continental Crust (UCC) and Depleted Mantle (N-MORB), their $^{87}Rb/^{86}Sr$ (UCC $^{87}Rb/^{86}Sr = 0.743$, and N-MORB, $^{87}Rb/^{86}Sr = 0.018$) are based on the concentrations of Rb and Sr in UCC and N-MORB recommended in Rudnick and Gao (2003) and Sun and McDonough (1989), respectively. (b) Whole rock ε_{Nd} vs. time (Ga) plot for mafic dykes of the Singhbhum Craton (Table 3). The Nd evolution arrays for the Paleoarchean Singhbhum granitoids and 3.5 Ga Depleted Mantle are from Pandey et al. (2019). The light blue arrows mark the secular isotopic evolution trend of the source of Singhbhum dykes. CHUR = Chondritic Uniform Reservoir.

average continental crust-like chondrite normalized REE patterns (Figs. 4a - d) and Primitive-Mantle normalized multi-element patterns (Figs. 4e - h) of the most primitive dykes (Mg# > 60; Table 2) suggest that the crust-like abundances of incompatible elements in these dykes are source characteristics as they require equilibration with a mantle mineralogy to account for the high abundances of compatible trace elements. Moreover, the $^{87}Sr/^{86}Sr_i$ and $\varepsilon_{Nd(i)}$ of dykes of all four swarms together define a crust-like growth trend (Fig. 5). This relationship and trend cannot be achieved through assimilation of felsic continental crust by the parental magmas at different times of emplacement of these different dyke swarms. Therefore, the crust-like incompatible trace element abundances (Figs. 3, 4) together with the Nd and Sr isotopes of the Singhbhum dykes that define a time-integrated growth-array (Fig. 5) are not the result of assimilation of

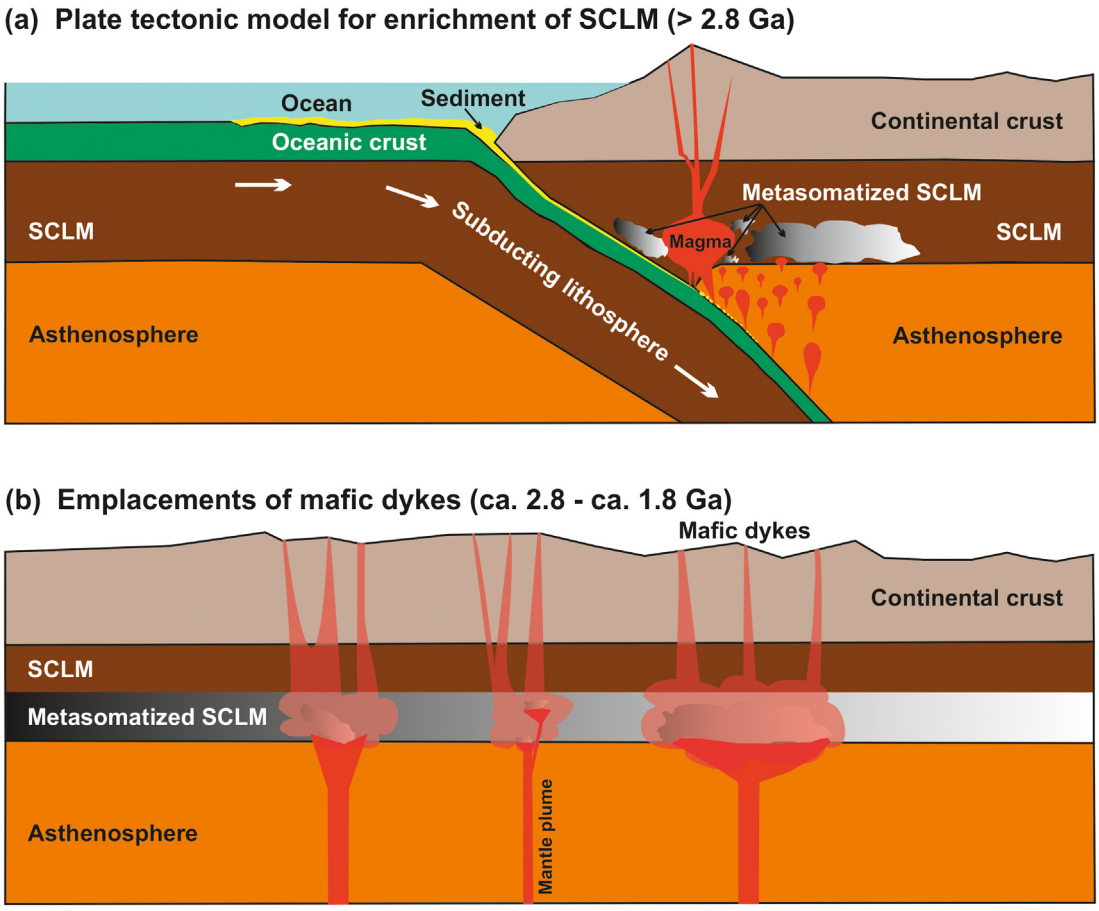

Fig. 6. Schematic diagram for (a) metasomatization of the subcontinental lithospheric mantle (SCLM) beneath the Singhbhum Craton by recycling of crustal material by subduction prior to 2.8 Ga, and (b) mantle plumes induced partial melting of the metasomatized SCLM leading to emplacements of mafic dykes between ca. 2.8 Ga and ca. 1.8 Ga.

felsic continental crust (at crustal depth) by the parental magmas during ascent, but inherited from their mantle source(s).

5.1.3. Ancient subduction driven metasomatism of SCLM

Our preferred explanation for the strong enrichment of incompatible elements (e.g., $La/Lu_N = 4.12 – 11.17$ for most of the Singhbhum Craton dykes, Figs. 4a - d; La/Lu_N of UCC = 10.72, Rudnick and Gao, 2003; La/Lu_N of average MORB = 1.05, Gale et al., 2013), relatively high abundance of compatible elements and negative Nb, Ta, and Ti anomalies particularly in the most primitive basaltic samples is that the melts were derived from an enriched mantle source. The enrichment must have happened in the mantle source to produce melts of basaltic composition enriched in compatible elements. This source could be a depleted mantle contaminated with crustal material (Fig. 6a; e.g., Karoo LIP in the southern Africa, and Wrangellia LIP in the Pacific; see pages 304 – 305 in Ernst, 2014). However, some dyke samples such as Kes 8 ($La/Lu_N = 2.32$) of the ca. 2.80 Ga swarm; Gha 5 ($La/Lu_N = 1.20$) and Gha 11 ($La/Lu_N = 1.74$) of the ca. 2.76 Ga swarm; and Kap 5 ($La/Lu_N = 1.77$), and Kap 8 ($La/Lu_N = 2.66$) of the ca. 2.26 Ga swarm, have nearly flat REE patterns (Figs. 4a - d), which suggest the presence of a depleted mantle (non-metasomatized) component in the source.

The compatible element abundances in the primitive members (with Mg# > 60) of the basaltic dykes indicate that the parental melts were in equilibrium with mantle peridotite. High Ni, Cr, and V concentrations and high Mg# of the most primitive dykes indicate that their parental magmas underwent none to little fractional crystallization. Further, a lack of strong depletion in HREE and insignificant negative Eu anomalies indicate a non-garnetiferous and plagioclase free source. Such a source that can produce basaltic melts with high concentration of transition elements would be a spinel lherzolite.

5.2. Source signatures from Sr-Nd isotopic compositions

The Sr and Nd isotopic ratios also indicate a heterogeneous sources for the parental magmas of these dyke swarms. The crust-like Sr and Nd isotope compositions (Fig. 5) of most of the dyke basalts record an enrichment of SCLM source prior to ca. 2.80 Ga (Fig. 6a). This interpretation is in agreement with Roy et al. (2004), who suggested a metasomatized mantle source for the origin of the ca. 2.80 Ga Keshargaria dyke swarm. The isotope composition of the basaltic melts and rocks of the Singhbhum Craton are consistent with metasomatism of the SCLM source through subduction contemporaneous with the emplacement of the granitoids of the Singhbhum Craton between ca. 3.47 and ca. 3.28 Ga (e.g., Pandey et al., 2019; Upadhyay et al., 2014). The trend of increasing $^{87}Sr/^{86}Sr_i$ and decreasing $\varepsilon_{Nd(i)}$ values with younger ages (Fig. 5) suggests incubation of enriched crustal material in the mantle source for a long time (>2.80 Ga to ca. 1.76 Ga). Partial melting of this mantle source periodically produced basaltic parental melts that were emplaced as dykes within the continental crust (Fig. 6b). The fact that the crustal component survived for such a long time in the mantle to generate enriched isotopic signatures observed in the Singhbhum dykes implies that it must have remained isolated from mantle convection. The older crustal material may have been introduced into the mantle by subduction and led to the metasomatization of the SCLM (Fig. 6a; e.g., Goodenough et al., 2002; Paul et al., 2020; Zhao and McCulloch, 1993). In a geological setting where an orogeny has occurred previously, mantle-derived melts intruding the overlying continental crust exhibit incompatible element abundances (e.g., LREE enriched chondrite normalized REE patterns; and negative Nb, Ta, and Ti anomalies in Primitive-Mantle normalized multi-element patterns) and isotope compositions (e.g., crust-like Nd

and Sr isotope ratios) similar to those of the continental crust in the region. These melts sample the upper mantle that was enriched by subduction-related processes during the orogenic cycle (e.g., Altherr et al., 2000). Although most of the Singhbhum dykes have crust-like $^{87}Sr/^{86}Sr_i$ and $\varepsilon_{Nd(i)}$, a few samples of the ca. 2.80 Ga swarm have depleted mantle-like $^{87}Sr/^{86}Sr_i$ and $\varepsilon_{Nd(i)}$ values (Fig. 5). This suggests that at least two components, namely depleted mantle and recycled crust, were involved in the petrogenesis of these dykes. The depleted-mantle component may represent, either depleted (non-metasomatized) portions of heterogeneous SCLM or depleted-mantle components in an impinging mantle plume (e.g., Fitton et al., 2003) that triggered partial melting of the SCLM.

5.3. Involvement of mantle plume(s)

Even if the dykes of the Singhbhum Craton do not exhibit typical OIB-like chondrite normalized REE and Primitive-Mantle normalized multi-element patterns (Fig. 4); their large areal extent (individual swarm lengths extending upto more than 100 km, and individual dyke width ranging between 50 and 500 m), parallel to sub-parallel as well as radial intrusion patterns of the dykes of individual swarms, and emplacement of each generation of the dyke swarm within short magmatic pulses, indicate that they are the plumbing systems of early-Neoarchean to late-Paleoproterozoic LIPs (e.g., Bryan and Ernst, 2008; Ernst, 2014). Additionally, these dykes are closely spaced in the southern part of the craton and become sparse towards the north. This radial pattern suggests that the dykes may be related to mantle plume (s) (e.g., Ernst, 2014; Ernst and Buchan, 1997). Therefore, the partial melting of enriched and heterogeneous SCLM may have been triggered multiple times between ca. 2.80 Ga and ca. 1.76 Ga by mantle plumes (Fig. 6b), leading to the emplacement of these mafic dyke swarms of different generations with different orientations but broadly similar major- and trace-element compositions and progressively more evolved Sr-Nd isotope compositions.

5.4. Correlation with dykes from other cratons

Based on the age and paleomagnetic data of mafic dyke swarms that were emplaced between ca. 2.8 Ga and ca. 1.8 Ga in several Archean cratons, the Singhbhum Craton can be placed into a larger paleogeographic framework. Similarities in the age of Archean to Paleoproterozoic dykes from other crustal blocks indicate spatial proximity of the Singhbhum Craton with the Bastar, Dharwar, North China, Pilbara, Kaapvaal, Zimbabwe, Amazonia, and Sarmatia Cratons as well as Antarctica in different configurations between ca. 2.8 Ga and ca. 1.8 Ga (e.g., Kumar et al., 2017; Liao et al., 2019; Shankar et al., 2014, 2018; Srivastava et al., 2019). However, compositional data for most dykes in this age range are missing. For ca. 2.36 Ga boninitic-noritic dykes of the neighboring cratons, Liao et al. (2019) reported $^{87}Sr/^{86}Sr_i$ ranging from 0.70145 to 0.70447 and $\varepsilon_{Nd(i)}$ −6.4 to +4.5 for Bhanupratappur mafic dykes, central Bastar Craton, and $^{87}Sr/^{86}Sr_i$ ranging from 0.701165 to 0.701633 and $\varepsilon_{Nd(i)}$ from −0.7 to +0.6 for Karimnagar mafic dykes, north Eastern Dharwar Craton. Pandey et al. (2020) reported $^{87}Sr/^{86}Sr_i = 0.70097 - 0.70506$ and $\varepsilon_{Nd(i)} = -2.7 - +0.85$ for ca. 2.36 Ga tholeiitic basalt to basaltic-andesite and boninitic-noritic dykes of the Bhanupratappur swarm, Bastar Craton. These results indicate that the Bhanupratappur dykes were derived from an isotopically heterogeneous source having both depleted and enriched components. In contrast, the Karimnagar dykes originated from an isotopically homogeneous source having chondritic composition. Han et al. (2015) argued that the ca. 2.24 Ga Zhaiwa mafic dykes of North China Craton, characterized by $^{87}Sr/^{86}Sr_i = 0.705605 - 0.748725$ and $\varepsilon_{Nd(i)} = -6.7$ to −3.3, were emplaced by asthenospheric upwelling-induced-melting of a SCLM source containing subducted crustal material. More isotopic data of contemporaneous (ca. 2.8 Ga – ca. 1.8 Ga) mafic dykes from other cratonic blocks are required to better constrain the lithospheric mantle characteristics during the Neoarchean-Paleoproterozoic.

6. Conclusions

The ca. 2.80 Ga to ca. 1.76 Ga tholeiitic to calc-alkaline basaltic to andesitic dykes of the Singhbhum Craton show inter- and intra-swarm elemental and isotopic heterogeneity. The high concentration of compatible trace elements, particularly Ni, Cr, and V, the high Mg# of the most primitive basaltic dykes, the lack of strong depletion of HREE, and insignificant negative Eu anomalies, indicate that the parental melt formed in equilibrium with a spinel lherzolite mantle source. The crust-like abundances of incompatible elements in most of the dyke rocks (including those with highest Mg#) indicate the derivation of parental melt from an enriched source. The presence of basalts with flat REE patterns and those with LREE enrichement attests to a chemically heterogeneous source. High concentrations of the transition elements in the primitive dykes, and crust-like REE and multi-element profiles of even the most primitive dykes exclude crustal assimilation (during magma ascent) as the cause for enrichment of parental magmas. Complementary to the trace elements, the $^{87}Sr/^{86}Sr_i$ and $\varepsilon_{Nd(i)}$ values of these dykes indicate a heterogeneous SCLM source. The source inherited an incompatible-element-enrichment (and crust-like Sr-Nd isotopes) signature during the Archean by incorporation of subducted crustal material. The mantle-derived melts preserved as dyke swarms provide indirect evidence for mantle enrichment processes contemporaneous with the genesis of continetal crust of the Singhbhum Craton during the Paleoarchean. The enriched SCLM source formed at that time was later periodically tapped (along with depleted-mantle components) during the thermal plume activities leading to multiple episodes of dyke formation over a period of 1 Gyr between the late-Archean and mid-Proterozoic.

Declaration of Competing Interest

The authors declare that they have no known competing financial interests or personal relationships that could have appeared to influence the work reported in this paper.

Acknowledgements

This work was supported by 'Swiss Government Excellence Scholarship (2014.0848)' and 'IIT Kanpur - Institute Postdoctoral Fellowship (PDF 156)' awarded to OPP. Alessandro Maltese and Mahesh Halder are thanked for their assistance during the field work. Hikari Kamioka is thanked for kindly sharing the JNdi-1 standard reference material. Rajesh Kumar Srivastava and Amiya Kumar Samal are thanked for sharing the vector file of the geological map of the Singhbhum Craton containing mafic dykes. Richard Ernst, Esa Heilimo, and Vladislav Rapprich are thanked for their suggestions which helped in improving the manuscript. Isotopes were measured on a Neptune Plus™ MC-ICP-MS acquired with funds from the NCCR PlanetS supported by the Swiss National Science Foundation (SNSF) grant nr. 51NF40-141881. Additional support was provided through the SNSF grant nr. 200021_160034. Constructive critical reviews by Angus Fitzpayne and an anonymous reviewer helped significantly in improving the manuscript. The efficient handling of the manuscript by the editor Michael Roden is also very much appreciated.

References

Aldanmaz, E., Köprübaşı, N., Gürer, Ö.F., Kaymakçı, N., Gourgaud, A., 2006. Geochemical constraints on the Cenozoic, OIB-type alkaline volcanic rocks of NW Turkey: implications for mantle sources and melting processes. Lithos 86, 50–76.

Altherr, R., Holl, A., Hegner, E., Langer, C., Kreuzer, H., 2000. High-potassium, calc-alkaline I-type plutonism in the European Variscides: northern Vosges (France) and northern Schwarzwald, Germany. Lithos 50, 51–73.

Anderson, E.M., 1951. The dynamics of faulting and dyke formation with application to Britain. 206. Oliver and Boyd Ltd., London, England.
Azizi, H., Stern, R.J., 2019. Jurassic igneous rocks of the central Sanandaj–Sirjan zone (Iran) mark a propagating continental rift, not a magmatic arc. Terra Nova 31, 415–423.
Azizi, H. and Stern, R.J., 2020. Reply to comment on Jurassic igneous rocks of the central Sanandaj–Sirjan zone (Iran) mark a propagating continental rift, not a magmatic arc. Azizi and Stern, Terra Nova 31(5), 415–423, 2019)", (32, 473-475).
Bartels, A., Nielsen, T.F., Lee, S.R., Upton, B.G., 2015. Petrological and geochemical characteristics of Mesoproterozoic dyke swarms in the Gardar Province, South Greenland: Evidence for a major sub-continental lithospheric mantle component in the generation of the magmas. Mineral. Mag. 79, 909–940.
Bleeker, W., 2004. Taking the pulse of planet Earth: a proposal for a new multi-disciplinary flagship project in Canadian solid Earth sciences. Geosci. Can. 31, 179–190.
Bose, M.K., 2009. Precambrian mafic magmatism in the Singhbhum craton, eastern India. J. Geol. Soc. India 73, 13–35.
Bouvier, A., Vervoort, J.D., Patchett, P.J., 2008. The Lu–Hf and Sm–Nd isotopic composition of CHUR: constraints from unequilibrated chondrites and implications for the bulk composition of terrestrial planets. Earth Planet. Sci. Lett. 273, 48–57.
Bryan, S.E., Ernst, R.E., 2008. Revised definition of large igneous provinces (LIPs). Earth Sci. Rev. 86, 175–202.
Buchan, K.L., Ernst, R.E., 2018. A giant circumferential dyke swarm associated with the High Arctic Large Igneous Province (HALIP). Gondwana Res. 58, 39–57.
Chandra, J., Paul, D., Stracke, A., Chabaux, F., Granet, M., 2019. The origin of carbonatites from amba dongar within the deccan large Igneous Province. J. Petrol. 60, 1119–1134.
de Kock, M.O., Ernst, R., Söderlund, U., Jourdan, F., Hofmann, A., Le Gall, B., Bertrand, H., Chisonga, B.C., Beukes, N., Rajesh, H.M., Moseki, L.M., 2014. Dykes of the 1.11 Ga Umkondo LIP, Southern Africa: clues to a complex plumbing system. Precambrian Res. 249, 129–143.
Dostal, J., Dupuy, C., Carron, J.P., De Kerneizon, M.L.G., Maury, R.C., 1983. Partition coefficients of trace elements: application to volcanic rocks of St. Vincent, West Indies. Geochimica et Cosmochimica Acta 47, 525–533.
Elahi-Janatmakan, F., Maghdour-Mashhour, R., Tabbakh Shabani, A.A., 2020. Comment on "Jurassic igneous rocks of the central Sanandaj–Sirjan zone (Iran) mark a propagating continental rift, not a magmatic arc'by Azizi and Stern (Terra Nova, 31 (5), 415-423, 2019)". Terra Nova 32, 468–472.
Ernst, R.E., Baragar, W.R.A., 1992. Evidence from magnetic fabric for the flow pattern of magma in the Mackenzie giant radiating dyke swarm. Nature 356, 511–513.
Ernst, R.E., Buchan, K.L.eds., 2001. Mantle plumes: their identification through time. Special Paper 352. Geological Society of America.
Ernst, R.E., Buchan, K.L., 1997. Giant radiating dyke swarms: their use in identifying pre-Mesozoic large igneous provinces and mantle plumes. Geophys. Monogr. Am. Geophys. Union 100, 297–334.
Ernst, R.E., 2014. Large igneous provinces. Cambridge University Press, p. 653.
Fitton, J.G., Saunders, A.D., Kempton, P.D., Hardarson, B.S., 2003. Does depleted mantle form an intrinsic part of the Iceland plume? Geochem. Geophys. Geosyst. 4.
French, J.E., Heaman, L.M., 2010. Precise U–Pb dating of Paleoproterozoic mafic dyke swarms of the Dharwar craton, India: implications for the existence of the Neoarchean supercraton Sclavia. Precambrian Res. 183, 416–441.
Frey, F.A., Green, D.H., Roy, S.D., 1978. Integrated models of basalt petrogenesis: a study of quartz tholeiites to olivine melilitites from south eastern Australia utilizing geochemical and experimental petrological data. J. Petrol. 19, 463–513.
Gale, A., Dalton, C.A., Langmuir, C.H., Su, Y., Schilling, J.G., 2013. The mean composition of ocean ridge basalts. Geochem. Geophys. Geosyst. 14, 489–518.
Goodenough, K.M., Upton, B.G.J., Ellam, R.M., 2002. Long-term memory of subduction processes in the lithospheric mantle: evidence from the geochemistry of basic dykes in the Gardar Province of South Greenland. J. Geol. Soc. 159, 705–714.
Gumsley, A., Olsson, J., Söderlund, U., de Kock, M., Hofmann, A., Klausen, M., 2015. Precise U-Pb baddeleyite age dating of the Usushwana Complex, southern Africa – Implications for the Mesoarchaean magmatic and sedimentological evolution of the Pongola Supergroup, Kaapvaal Craton. Precambrian Res. 267, 174–185.
Halls, H.C., 1982. The importance and potential of mafic dyke swarms in studies of geodynamic processes. Geosci. Can. 9, 145–154.
Han, J., Chen, H., Yao, J., Deng, X., 2015. 2.24 Ga mafic dykes from Taihua Complex, southern Trans-North China Orogen, and their tectonic implications. Precambrian Res. 270, 124–138.
Hasse, K.M., Goldschmidt, B., Garbe-Schönberg, C.D., 2004. Petrogenesis of Tertiary Continental Intra-plate Lavas from the Westerwald Region, Germany. Journal of petrology 45, 883–905. https://doi.org/10.1093/petrology/egg115.
Irvine, T.N.J., Baragar, W.R.A.F., 1971. A guide to the chemical classification of the common volcanic rocks. Can. J. Earth Sci. 8, 523–548.
Johannsen, A., 1931. A Descriptive Petrography of the Igneous Rocks: Introduction, textures, classifications, and glossary. University of Chicago Press.
Klemme, S., Günther, D., Hametner, K., Prowatke, S., Zack, T., 2006. The partitioning of trace elements between ilmenite, ulvospinel, armalcolite and silicate melts with implications for the early differentiation of the moon. Chem. Geol. 234, 251–263.
Kumar, A., Parashuramulu, V., Shankar, R., Besse, J., 2017. Evidence for a Neoarchean LIP in the Singhbhum craton, eastern India: Implications to Vaalbara supercontinent. Precambrian Res. 292, 163–174.
Kumar, K.V., Rathna, K., 2008. Geochemistry of the mafic dykes in the Prakasam Alkaline Province of Eastern Ghats Belt, India: implications for the genesis of continental rift-zone magmatism. Lithos 104, 306–326.
Le Maitre, R.W., Bateman, P., Dudek, A., Keller, J., Lameyre, J., Le Bas, M.J., Sabine, P.A., Schmid, R., Sorensen, H., Streckeisen, A., Woolley, A.R. & Zanettin, B., 1989: A Classification of Igneous Rocks and Glossary of Terms: Recommendations of the International Union of Geological Sciences Subcommission on the Systematics of Igneous Rocks. Blackwell Scientific Publications, Oxford.
Le Maitre, R.W., Streckeisen, A., Zanettin, B., Le Bas, M.J., Bonin, B., Bateman, P.eds., 2002. Igneous rocks: a classification and glossary of terms. Recommendations of the International Union of Geological Sciences Subcommission on the Systematics of Igneous Rocks, 2nd edn 236. Cambridge University Press.
Liao, A.C.Y., Shellnutt, J.G., Hari, K.R., Denyszyn, S.W., Vishwakarma, N., Verma, C.B., 2019. A petrogenetic relationship between 2.37 Ga boninitic dyke swarms of the Indian Shield: Evidence from the Central Bastar Craton and the NE Dharwar Craton. Gondwana Res. 69, 193–211.
Mukhopadhyay, D., 2001. The Archaean nucleus of Singhbhum: the present state of knowledge. Gondwana Res. 4, 307–318.
Pandey, O.P., Mezger, K., Ranjan, S., Upadhyay, D., Villa, I.M., Nägler, T.F., Vollstaedt, H., 2019. Genesis of the Singhbhum Craton, eastern India; implications for Archean crust-mantle evolution of the Earth. Chem. Geol. 512, 85–106.
Pandey, O.P., Mezger, K., Söderlund, U., Upadhyay, D., Srivastava, R.K., Gautam, G.C., Ernst, R.E., 2020. Geochronology, whole-rock geochemistry and Sr-Nd isotopes of the Bhanupratappur mafic dyke swarm: evidence for a common Paleoproterozoic LIP event at 2.37-2.36 Ga in the Bastar and Dharwar cratons. Precambrian Res. 347, 105853.
Papanastassiou, D.A., Wasserburg, G.J., 1969. Initial strontium isotopic abundances and the resolution of small time differences in the formation of planetary objects. Earth Planet. Sci. Lett. 5, 361–376.
Paul, D., Chandra, J., Halder, M., 2020. Proterozoic alkaline rocks and carbonatites of peninsular india: a review. Episodes J. Int. Geosci. 43, 249–277.
Pearce, J.A., 1996. A user's guide to basalt discrimination diagrams. Trace element geochemistry of volcanic rocks: applications for massive sulphide exploration. Geological Association of Canada, Short Course Notes. 12, p. 113.
Pearce, J.A., 2008. Geochemical fingerprinting of oceanic basalts with applications to ophiolite classification and the search for Archean oceanic crust. Lithos 100, 14–48.
Perfit, M.R., Gust, D.A., Bence, A.E., Arculus, R.J., Taylor, S.R., 1980. Chemical characteristics of island-arc basalts: implications for mantle sources. Chem. Geol. 30, 227–256.
Pradhan, V.R., Meert, J.G., Pandit, M.K., Kamenov, G., Mondal, M.E.A., 2012. Paleomagnetic and geochronological studies of the mafic dyke swarms of Bundelkhand craton, central India: implications for the tectonic evolution and paleogeographic reconstructions. Precambrian Res. 198, 51–76.
Ratre, K., De Waele, B., Biswal, T.K., Sinha, S., 2010. SHRIMP geochronology for the 1450 Ma Lakhna dyke swarm: Its implication for the presence of Eoarchaean crust in the Bastar Craton and 1450–517 Ma depositional age for Purana basin (Khariar), Eastern Indian Peninsula. J. Asian Earth Sci. 39, 565–577.
Reid, F., 1983. Origin of the rhyolitic rocks of the Taupo Volcanic Zone, New Zealand. J. Volcanol. Geotherm. Res. 15, 315–338.
Roy, A., Sarkar, A., Jeyakumar, S., Aggrawal, S.K., Ebihara, M., Satoh, H., 2004. Late Archaean mantle metasomatism below eastern Indian craton: Evidence from trace elements, REE geochemistry and Sr—Nd—O isotope systematics of ultramafic dykes. J. Earth Syst. Sci. 113, 649–665.
Rudnick, R.L., Gao, S., 2003. Composition of the continental crust. Treatise Geochem. 3, 659.
Saha, A.K., 1994. Crustal evolution of Singhbhum-North Orissa, Eastern India. Memoirs Geol. Soc. India 27, 341.
Sarkar, S.N., Saha, A.K., Miller, J.A., 1969. Geochronology of the Pre-Cambrian rocks of Singhbhum and adjacent regions, eastern India. Geol. Magazine 106, 15–45.
Sengupta, P., Ray, A., 2012. Newer Dolerite dykes, Jharkhand, India: a case study of magma generation, differentiation and metasomatism in a subduction zone setting. Geochem. J. 46, 477–491.
Sengupta, P., Ray, A., Pramanik, S., 2014. Mineralogical and chemical characteristics of newer dolerite dyke around Keonjhar, Orissa: Implication for hydrothermal activity in subduction zone setting. J. Earth Syst. Sci. 123, 887–904.
Sensarma, S., Paul, D., Rao, N.C., 2013. Large igneous provinces–global perspectives and prospects in India. Curr. Sci. 105, 182–192.
Shankar, R., Sarma, D.S., Babu, N.R., Parashuramulu, V., 2018. Paleomagnetic study of 1765 Ma dyke swarm from the Singhbhum Craton: Implications to the paleogeography of India. J. Asian Earth Sci. 157, 235–244.
Shankar, R., Vijayagopal, B., Kumar, A., 2014. Precise Pb–Pb baddeleyite ages of 1765 Ma for a Singhbhum 'newer dolerite'dyke swarm. Curr. Sci. 106, 1306–1310.
Sobolev, A.V., Hofmann, A.W., Kuzmin, D.V., Yaxley, G.M., Arndt, N.T., Chung, S.L., Danyushevsky, L.V., Elliott, T., Frey, F.A., Garcia, M.O., Gurenko, A.A., 2007. The amount of recycled crust in sources of mantle-derived melts. Science 316, 412–417.
Srivastava, R.K., Söderlund, U., Ernst, R.E., Mondal, S.K., Samal, A.K., 2019. Precambrian mafic dyke swarms in the Singhbhum craton (eastern India) and their links with dyke swarms of the eastern Dharwar craton (southern India). Precambrian Res. 329, 5–17.
Stracke, A., Scherer, E.E., Reynolds, B.C., 2014. 15.4 – Application of isotope dilution in geochemistry. In: Holland, H.D., Turekian, K.K. (Eds.), Treatise on Geochemistry, second ed. Elsevier, Oxford, pp. 71–86.
Sun, S.S., McDonough, W.S., 1989. Chemical and isotopic systematics of oceanic basalts: implications for mantle composition and processes. Geol. Soc. Lond., Spec. Publ. 42, 313–345.
Tanaka, T., Togashi, S., Kamioka, H., Amakawa, H., Kagami, H., Hamamoto, T., Yuhara, M., Orihashi, Y., Yoneda, S., Shimizu, H., Kunimaru, T., 2000. JNdi-1: a neodymium isotopic reference in consistency with LaJolla neodymium. Chem. Geol. 168, 279–281.
Thompson, R.N., Ottley, C.J., Smith, P.M., Pearson, D.G., Dickin, A.P., Morrison, M.A., Leat, P.T., Gibson, S.A., 2005. Source of the quaternary alkalic basalts, picrites and basanites of the Potrillo Volcanic Field, New Mexico, USA: lithosphere or convecting mantle? J. Petrol. 46, 1603–1643.

Upadhyay, D., Chattopadhyay, S., Mezger, K., 2019. Formation of Paleoarchean-Mesoarchean Na-rich (TTG) and K-rich granitoid crust of the Singhbhum craton, eastern India: constraints from major and trace element geochemistry and Sr-Nd-Hf isotope composition. Precambrian Res. 327, 255–272.

Upadhyay, D., Chattopadhyay, S., Kooijman, E., Mezger, K., Berndt, J., 2014. Magmatic and metamorphic history of Paleoarchean tonalite–trondhjemite–granodiorite (TTG) suite from the Singhbhum craton, eastern India. Precambrian Res. 252, 180–190.

Villa, I.M., De Bièvre, P., Holden, N.E., Renne, P.R., 2015. IUPAC-IUGS recommendation on the half-life of 87Rb. Geochim. Cosmochim. Acta 164, 382–385.

Wang, Y., Fan, W., Zhang, Y., Guo, F., Zhang, H., Peng, T., 2004. Geochemical, $^{40}Ar/^{39}Ar$ geochronological and Sr–Nd isotopic constraints on the origin of Paleoproterozoic mafic dikes from the southern Taihang Mountains and implications for the ca. 1800Ma event of the North China Craton. Precambrian Res. 135, 55–77.

Wood, D.A., 1980. The application of a Th-Hf-Ta diagram to problems of tectonomagmatic classification and to establishing the nature of crustal contamination of basaltic lavas of the British Tertiary Volcanic Province. Earth Planet. Sci. Lett. 50, 11–30.

Zhang, J., Guo, P., Sun, P., Niu, Y., Xiao, Y., Vasconcelos, P.M., 2020. Petrogenesis of the early Cretaceous intra-plate basalts from the Western North China Craton: Implications for the origin of the metasomatized cratonic lithospheric mantle. Lithos, 105887 https://doi.org/10.1016/j.lithos.2020.105887.

Zhao, J.X., McCulloch, M.T., 1993. Melting of a subduction-modified continental lithospheric, mantle: Evidence from Late Proterozoic mafic dike swarms, in central Australia. Geology 21, 463–466.

Zindler, A., Hart, S., 1986. Chemical geodynamics. Annu. Rev. Earth Planet. Sci. 14, 493–571.